THESIS FOR THE DEGREE OF DOCTOR OF PHILOSOPHY

Mesoscopic phenomena in the electromechanics of suspended nanowires

GUSTAV SONNE

GÖTEBORGS UNIVERSITET

Department of Physics
University of Gothenburg
SE-412 96 Göteborg, Sweden 2011

Mesoscopic phenomena in the electromechanics of suspended nanowires
GUSTAV SONNE
ISBN: 978-91-628-8244-0
Electronic version available at:
http://hdl.handle.net/2077/24289

Doktorsavhandling vid Göteborgs Universitet

Condensed Matter Theory Group
Department of Physics
University of Gothenburg
SE-412 96 Göteborg
Sweden
Telephone +46 (0)31 786 0000

Typeset in LaTeX

Figures created using MATLAB, Inkscape, CorelDRAW and POV-Ray

All figures presented in the thesis are the original work of the author unless otherwise stated

Printed by Chalmers Reproservice
Chalmers University of Technology
Göteborg, Sweden 2011

Mesoscopic phenomena in the electromechanics of suspended nanowires

GUSTAV SONNE
Condensed Matter Theory
Department of Physics
University of Gothenburg

ABSTRACT

Over the last two decades nanotechnology has been a very active field of scientific research, both from fundamental perspectives as well as for applications in technology and consumer goods. In this thesis, theoretical work on quantum mechanical effects on charge transport in nanoelectromechanical systems is presented. In particular, the effects of electron-vibron interactions in suspended nanowire structures are analysed and discussed.

The thesis is structured around the appended scientific publications by the author. Also included is an introductory section where the underlying theory and motivation is presented. This introduction forms the basis on which the subsequent material and appended papers is based.

The work presented in the appended papers considers systems comprising suspended oscillating nanowires, primarily in the form of carbon nanotubes. Central to these studies is the interaction between the charge transport and the mechanical motion of the nanowires. For the systems analysed in this thesis, these interactions are mediated through transverse magnetic fields, the effect of which is studied in various system setups. In particular, three topics of mesoscopic phenomena are presented; i) a temperature-independent current deficit due to interference effects between different electronic tunnelling paths over the nanowire-junction, ii) pumping of the mechanical vibrations in a low transparency superconducting junction, and iii) cooling of the mechanical vibrations in both current- and voltage-biased superconducting junctions.

The outcome of the presented work is a number of interesting physical predictions for the electromechanics of suspended nanowires. These results are shown to be experimentally observable in systems with high mechanical resonance frequencies and if sufficiently strong electromechanical coupling can be achieved. Once these conditions are fulfilled, the predicted results are of interest both from a fundamental perspective in that they probe the underlying quantum nature of the systems, but also for sensing applications where quantum limited resolution could be experimentally achievable.

Keywords: Nanoelectromechanical systems, ground-state cooling, superconducting weak links, carbon nanotubes, non-linear resonance,

Research publications

This thesis is an introduction to and summary of the work published in the following research articles, which are appended. These are referred to as Paper I-IV.

PAPER I

Temperature-independent current deficit due to induced quantum nanowire vibrations
G. Sonne
New Journal of Physics **11**, 073037 (2009)

PAPER II

Superconducting pumping of nanomechanical vibrations
G. Sonne, L. Y. Gorelik, S. I. Kulinich, R. I. Shekhter and M. Jonson
Physical Review B **78**, 144501 (2008)

PAPER III

Cooling of a Suspended Nanowire by an ac Josephson Current Flow
G. Sonne, M. E. Peña-Aza, L. Y. Gorelik, R. I. Shekhter and M. Jonson
Physical Review Letters **104**, 226802 (2010)

PAPER IV

Ground-state cooling of a suspended nanowire through inelastic macroscopic quantum tunneling in a current-biased Josephson junction
G. Sonne and L. Y. Gorelik
arXiv:1101.0531 (2011)
Submitted to Physical Review Letters

These papers are appended at the end of the thesis.

Related scientific work by the author not included in the thesis

Quantum Mechanical Effects on Charge Transport in Two Mesoscopic Systems
G. Sonne
Licentiate thesis, University of Gothenburg (2008)

High-temperature excess current and quantum suppression of electronic backscattering
G. Sonne, L. Y. Gorelik, R. I. Shekhter and M. Jonson
Europhysics Letters **84**, 27002 (2008)

Nonequilibrium and quantum coherent phenomena in the electromechanics of suspended nanowires
R. I. Shekhter, F. Santandrea, G. Sonne, L. Y. Gorelik and M. Jonson
Low Temperature Physics **35**, 662 (2009)

Voltage-driven superconducting weak link as a refrigerator for cooling of nanomechanical vibrations
G. Sonne, M. E. Peña-Aza, L. Y. Gorelik, R. I. Shekhter and M. Jonson
Low Temperature Physics **36**, 902 (2010)

Preface

Since the autumn of 2006 I have been working as a graduate student in the Condensed Matter Theory group at the Department of Physics at the University of Gothenburg. The material presented in this PhD thesis is a summary of my work over these years, which has primarily focused on the effects of electromechanical interactions in suspended nanowire structures.

The thesis consists of two parts. The most important part is the scientific papers, referred to as Paper I-IV, which are appended at the end of the thesis. The second part of the thesis consists of an introduction to the topics discussed in the papers. In this section I aim to familiarise the reader with the field in which I have been active during my PhD studies, as well as to include some background material to the topics covered in the appended papers. It is my intention and hope that this section should, at least in part, be accessible to readers who may not have a background in physics. In particular I have written this section with my family and friends in mind with the hope that they will be able to appreciate and understand what I have been doing these years.

It may so happen that the experienced physicist will find the introductory discussion to this thesis somewhat trivial and prosaic. Should this be the case, I would like to add that to me, doing research is not only about getting interesting scientific results. Equally important is our ability to promote our knowledge to a wider audience than the world of academia. Hopefully I have been able to do so here.

The outline of the thesis is as follows. In Chapter 1, I give a short introduction to the field of nanotechnology and nanoelectromechanical systems. Chapter 2 presents a brief introduction to quantum mechanics where particular emphasis is put on the quantum harmonic oscillator, which forms an intricate part of the work presented in this thesis. Also, cooling of mechanical oscillators is discussed. In Chapter 3 the reader is introduced to some phenomena related to superconductivity. Similarly, Chapter 4 gives a short introduction to carbon nanotubes and some of their basic mechanical and electronic properties. In Chapter 5, the work of the appended papers is introduced and summarised. This chapter is somewhat more technical in its presentation, although I have tried to keep the mathematical formalism to a minimum. Finally, I conclude the thesis in Chapter 6 where I summarise the most important

results of my research.

TABLE OF CONTENTS

CHAPTER 1

Introduction

“I would like to describe a field, in which little has been done, but in which an enormous amount can be done in principle. [...] it would have an enormous number of technical applications. What I want to talk about is the problem of manipulating and controlling things on the small scale.” [1]

The above quote is taken from Richard Feynman’s lecture at the American Physical Society meeting in 1959 where he coined the phrase "there’s plenty of room at the bottom". In this seminal talk Feynman challenged his contemporaries to think outside (or perhaps inside) the box and ask themselves what sets the physical limits to how small we can make things. Many of the questions and challenges raised in this lecture, at the time seen as dubious, are today at the front line of technological research thanks primarily to improvements in fabrication- and microscopy-techniques at the very small scale. This emerging field, nanotechnology, has over the last two decades received a tremendous amount of scientific and economic interest. So much so that it has been coined "the next industrial revolution".

1.1 Nanotechnology

Nanotechnology is a term which incorporates a vast field of scientific and technological applications. The word derives from the Greek word "nano" (meaning dwarf) and is attributed to manipulations on the nano-to micrometre length scale ($10^{-9} - 10^{-6}$ m). At these scales physical objects behave very differently from their macroscopic counterparts, something which nanotechnological manufacturers wish to utilise. Some examples of this is that elements may go from being metallic opaque to transparent (e.g. copper) or take on catalytic properties (e.g. gold) as their dimensions are reduced. Furthermore, physical interactions between objects change as their size go down, resulting in microscopic phenomena that are not seen on the larger scale. Many of these effects can be attributed to the large surface to volume ratio at the nanoscale. Put simply, when an object is very small, proportionally more of its atoms will be on the surface as compared to a larger version of the same object. As surface atoms are very important in many physical and chemical reactions, having proportionally more surface atoms often means that new

physical phenomena are to be expected.

Applications of nanotechnology are today becoming more and more abundant with the number of nanotechnological products on the market having grown by an impressive 379% between 2006 and 2009 [2]. To date, most of these products are what would be called passive applications, e.g. nanoparticles used in cosmetics or for structural reinforcement purposes. However, more complex systems, where nanometre-sized objects are of necessity for the product to function properly, are emerging. A potentially very lucrative field for nanotechnological applications is for example electronics where nanometre-sized components could significantly decrease both energy consumption and heat production [3].

In order for systems as small as a few tens of nanometres to work properly, control on the atomic scale is needed in their manufacturing. This is doubtlessly the biggest challenge facing nanotechnology at the moment. In essence it boils down to pin-pointing the position of only a few atoms or molecules accurately enough that the object you are creating will be able to perform the desired operation in a repeated fashion over a long period of time. Nature has of course solved this problem long ago, as the molecules and proteins that make up living life are found on the nanometre length scale. Manipulation of objects this small is thus by no means impossible. The question is only how to do it in a controlled way. Once such control is attainable in a repeated and traceable fashion we may not be too far away from realising Feynman's 50-year old vision.

1.2 Physics at the nanoscale

Everyday objects are described through Newton's laws of motion which describe the macroscopic world we inhabit. On the other hand microscopic objects, molecules, atoms and electrons are described through the laws of quantum mechanics. Both descriptions work exceedingly well for the processes they aim to describe and we believe both to be correct. However, Newtonian mechanics fails to accurately describe the world of atoms; just as a quantum description of a child on a swing would make little sense. Thus, we believe both ways of describing the world to be correct, but that their region of validity is bound by the size of the objects being considered.

For length scales in-between the micro- and macroscopic regimes an overlap between these disparate laws of nature is needed. This regime, often called the mesoscopic scale (the word "meso" being Greek for in intermediate), is exactly the scale at which nanotechnological applications reside. Mesoscopic systems typically consist of millions of atoms. Therefore, a complete quantum mechanical description of the system becomes mathematically unwieldy and scientists have to resort to sagacious approximations to reduce the complexity

of the problem. Such approximations often involve some averaging over for example the discrete atomic structure, without losing sight of the underlying physics governing the system. As an example, the suspended nanowire structures considered in the latter chapters of this thesis are often treated quantum mechanically. Here, a wire a few hundred nanometres long is considered as one single quantum object. This is of course a big generalisation as the wire consists of thousands of atoms. However, from a macroscopic perspective we know that we can describe the atoms in the wire as single object, and by extending this analysis to the quantum world we can often substitute the motion of each atom by the generalised motion of the wire without losing sight of the underlying physical properties of the system (in this case the nanowire).

The present thesis primarily focuses on nanoelectromechanical systems. These are systems where objects on the nanoscale are made to perform mechanical oscillations which are coupled to the motion of electrons through them. Seeing that the mechanically compliant objects considered are very small and that the frequency with which they oscillate is very high, we can describe them in the language of quantum mechanics. Thus, we expect these systems to react differently to external stimuli as compared to their macroscopic counterparts, something which one wishes to utilise for applicational purposes.

1.2.1 Nanoelectromechanical systems

Physical phenomena are described through the degrees of freedom accessible to the system, e.g. a ball thrown into the air has mechanical degrees of freedom and can be described through Newton's laws of motion. By coupling different degrees of freedom, systems can be made to respond to external stimuli in novel ways.

Coupling between mechanical and electrical degrees of freedom was perhaps first shown by William Gilbert in the late 16th century with his invention of the electroscope. With his device — a pivoted needle which could deflect due to the presence of charged objects — Gilbert was one of the first to study the interaction between electronic (the charged objects) and mechanical (the deflection of the needle) degrees of freedom. Since then, numerous applications utilising this type of coupling have seen the light of day.

Today, microelectromechanical systems, which build on the same principles as Gilbert's electroscope, are used for a plethora of applications, e.g. micrometer-sized accelerometers for airbags and gyroscopes for various stabilisation purposes. Common to these is that they use the mechanical properties of the system to influence the electronic read-out. As an example, the accelerometer in an airbag has a mechanical component which reacts when the car decelerates quickly, thus stimulating an electronic signal which releases the airbag.

Nanoelectromechanical systems are the smaller cousin of micromechanical systems. These nanometre-sized "machines" are envisaged not only to continue our strive for the smaller and faster components, but are also hoped to offer unprecedented measurement sensitivity. Examples of this include ultrasensitive mass detection using nanoscale oscillators with the possibility of resolutions down to individual molecules or atoms [4–7]. Another promising application is the magnetic resonance force microscope which enables mapping of electronic and nuclear spins at a resolution which greatly surpasses that of traditional magnetic resonance imaging. For a review on the operation, potential applications and challenges facing nanoelectromechanical systems the reader is referred to Refs. [8–10].

The reason why nanoscale systems are so sensitive to external stimuli derives from their reduced size. Typically, the frequency ω at which a mechanical resonator oscillates scales inversely with its dimensions. Decreasing the size of the oscillator thus implies increasing the mechanical frequency. Typical resonance frequencies for nanomechanical oscillators are in the radio frequency range (100 kHz to 10 GHz) which allows for very fast responses to external forces. Also, these systems often have high mechanical quality factors (a measurement of the sensitivity of the oscillator to perturbations) which implies that the weight of an extra atom should in principle be enough to sufficiently change the vibrations of a high-quality nanoelectromechanical oscillator such that the effect would be detectable.

CHAPTER 2

Quantum mechanics

The material presented in this thesis is based on the effects of electromechanical coupling in systems where an oscillating suspended nanowire forms the mechanically compliant element. In much of the following analysis the suspended nanowire is considered in the language of quantum mechanics. This chapter thus aims to give a short introduction to the physics of the quantum harmonic oscillator and the concept of ground-state cooling.

2.1 The quantum harmonic oscillator

The most simple and widely studied object in physics is the harmonic oscillator. Virtually any object which performs periodic motion around a central position can be described as a harmonic oscillator, e.g. a pendulum, a bridge resonating under the marching of soldiers over it or the relative motions of atoms in molecules. Also, the transverse oscillations of the suspended nanowires considered here can be described in this language. A diagram of a typical device geometry of the nanoelectromechanical systems considered in this thesis is shown in Fig. 2.1 where the suspended nanowire is free to vibrate just like a plucked guitar string.

Mathematically a classical harmonic oscillator, such as a mass on a spring, is described by the equation,

$$\frac{mv^2}{2} + \frac{kx^2}{2} = E\,. \tag{2.1}$$

In the above, m is the mass of the object, v is its velocity, k the spring constant which acts to pull the object back towards the centre and x is its coordinate of deflection. The above equation simply tells us that when the oscillator moves fast it has high kinetic energy and its potential energy is low. Similarly, close to the turning points the potential energy is large (x is large) whereas the kinetic energy is low. Throughout this process the total energy E is conserved. Also, the energy of classical harmonic oscillator may take any value as this is simply determined by how far the oscillator deflects from the central position. Similarly, if the oscillator performs no motion, its total energy is 0. Quantum mechanically things are different.

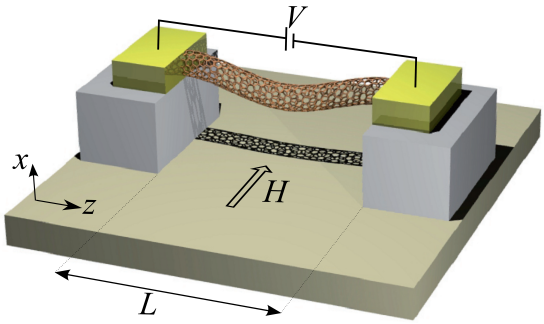

Figure 2.1: Schematic diagram of a nanowire oscillator considered in the thesis. A wire of length $L = 100\,\text{nm}$ — $1\,\mu\text{m}$ is suspended between two leads. In the above geometry, the actuation of the wire derives from the coupling between the current through the nanowire and the transverse magnetic field H.

The motion of the quantum harmonic oscillator is described through the Schrödinger equation,

$$\hat{H}|n\rangle = \left(\frac{\hat{p}^2}{2m} + \frac{1}{2}m\omega^2\hat{x}^2\right)|n\rangle = E_n|n\rangle\,, \tag{2.2}$$

for the energy eigenstate $|n\rangle$. This equation is nothing but the quantum equivalent of equation (2.1), i.e. it describes the same physical processes, but in the language of quantum mechanics. In the above, $\omega = \sqrt{k/m}$ is the frequency at which the oscillator vibrates, $\hat{p}$ is the momentum operator and $\hbar$ is the reduced Planck constant. Solving equation (2.2) one finds that the energy of the quantum harmonic oscillator is not free to take any value. Rather, the energy of the oscillator can only take the values $E_n = \hbar\omega(n+1/2)$ where $n = 0, 1, 2, ...$ Thus, we say that the energy levels of the quantum harmonic oscillator are quantised as they can only be found at multiples of the natural energy scale of the oscillator $\hbar\omega$. Furthermore, even at $n = 0$ the energy of the oscillator is not 0 but $\hbar\omega/2$. This is not surprising as things can never be perfectly still in quantum mechanics. Even at zero temperature, things vibrate with an amplitude which is known as the zero-point amplitude. It is these vibrations which give the oscillator energy, even if it is in the ground state $n = 0$.

Quantum mechanics is a probabilistic theory. This means that we can only talk about the probability $P(n)$ of finding the oscillator in a given state $|n\rangle$ with energy E_n. For a harmonic oscillator in thermal equilibrium this probability is dictated by the temperature T according to,

$$P(n) = e^{-n\hbar\omega/k_BT}\left(1 - e^{-\hbar\omega/k_BT}\right)\,, \tag{2.3}$$

where k_B is the Boltzmann constant. The above implies that at low temperatures ($\hbar\omega \gg k_BT$) the probability of finding the oscillator in the ground state $n = 0$ is high, whereas the probability of finding it in higher states is

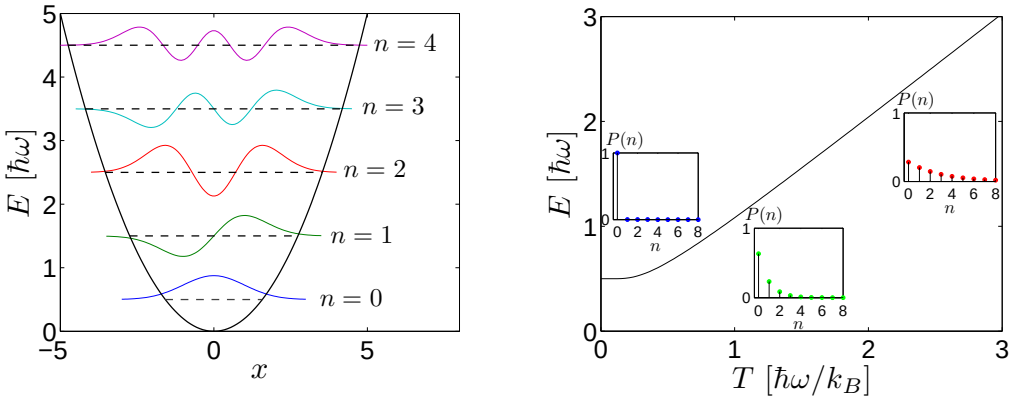

(a) (b)

Figure 2.2: (a) Energy levels and the corresponding wave functions for the 5 lowest eigenstates of the quantum harmonic oscillator. In the above, E is the energy in units of $\hbar\omega$ and x is the deflection in arbitrary units. For the quantum oscillator the lowest possible energy, the ground state energy, is $\hbar\omega/2$. The equivalent classical oscillator, e.g. a ball rolling in the potential shown by the solid line, can on the other hand be found at any energy depending on how far it deflects from $x = 0$. (b) The average energy of a quantum harmonic oscillator as a function of the temperature. In the low temperature limit, the ground state energy $\hbar\omega/2$ is achieved, whereas the energy of the oscillator scales with the temperatures in the opposite limit. The insets show the probability of finding the oscillator in the state n for three different temperatures, $k_BT/\hbar\omega = 1/10, 1, 3$. Here, the blue dots correspond to ground-state cooling $P(n = 0) \simeq 1$ where the oscillator is found in the state $n = 0$ with close to unit probability.

much lower. In Fig. 2.2(a) the energy levels and wave functions for the 5 lowest energy states of a quantum harmonic oscillator is shown. Also plotted is the average energy of the oscillator as a function of the temperature and the corresponding distribution of the population of the vibrational modes $P(n)$, Fig. 2.2(b).

Seeing that the state of the oscillator can only be found at discrete, equidistant, quantised energy levels one may describe it in terms of creation $\hat{b}^\dagger$ and annihilation $\hat{b}$ operators. These are objects which induce changes in the distribution of the population of the vibrational modes of the oscillator. In particular, their construction is such that when acting on the energy eigenstate $|n\rangle$ they move the system to the energy state above/below,

$$\hat{b}^\dagger|n\rangle = \sqrt{n+1}|n+1\rangle\,, \qquad \hat{b}|n\rangle = \sqrt{n}|n-1\rangle\,. \tag{2.4}$$

With this description, equation (2.2) could equally well be written as $\hat{H} = \hbar\omega(\hat{b}^\dagger\hat{b} + 1/2)$, which is the form most often used in the attached papers. Also, the creation and annihilation operators are related to the position operator $\hat{x}$ (see equation (2.2)) according to $\hat{x} = x_0(\hat{b} + \hat{b}^\dagger)$ where $x_0 = \sqrt{\hbar/(2m\omega)}$ is the

zero-point amplitude.

As the operator $\hat{b}$ always lowers the state of the system by one energy quantum, applying it many times corresponds a successive reduction of the number of the state (applying $\hat{b}^\dagger$ does the opposite). Thus, the operation $\hat{b}$ corresponds to shifting the probability distribution $P(n)$ to lower n. Considering that the "effective" temperature of the oscillator is defined by its probability distribution according to (2.3), the action of the operator $\hat{b}$ thus corresponds to a lowering of the "effective" temperature of the oscillator below that of the surrounding medium. This is the underlying mechanism behind cooling as discussed further in Section 2.3.

2.2 Classical physics meets quantum mechanics

High frequency nanometre-sized mechanical oscillators like those discussed in Chapter 1 are not only attractive for their high sensitivity to external perturbations. They also open up the possibility to probe quantum mechanical effects in a domain not previously accessible.

Crudely speaking, an object is considered to be in the quantum regime (such that any measurement on it will have a probabilistic outcome governed by quantum mechanics) if its associated frequency is higher than the temperature at which the experiment is performed, $\hbar\omega \gg k_B T$. Relating back to the previous section, this limit corresponds to a distribution of the vibrational modes of the oscillator $P(n)$ with only the few lowest modes populated. Whenever this applies, thermal fluctuations from the surrounding thermal bath are much smaller than the intrinsic quantum noise associated with any measurement. Under such conditions, experimental observations of discrete quantum transitions on the oscillator should be possible. Achieving this in a controlled way would present an exciting new arena for technological applications ultimately governed by the laws of quantum mechanics. Or, in the words of Keith Schwab and Michael Roukes, achieving this limit means that we are "approaching [...] an era when mechanical engineers will have to include $\hbar$ among their list of standard engineering constants." [11].

Seeing that the frequency of an oscillator scales inversely with its size one may question whether sub-micron-sized oscillators can be manufacturing so that the quantum limit is achievable at low temperatures. Indeed this is the case, as recently demonstrated by O'Connell and colleagues who succeeded in putting a 6 GHz macroscopic oscillator in its quantum mechanical ground state by cooling it to 25 mK in a dilution refrigerator [12].[1]

The mechanical frequencies of most oscillators considered to date are how-

[1] Note that the quoted frequency refers to the temporal frequency f and not the angular frequency $\omega = 2\pi f$ mostly used in this thesis.

ever substantially lower. As an example, a typical Si- or GaAs beam oscillator a few hundred nanometres long will have a natural frequency of its fundamental mode of $\omega \sim 100\,\mathrm{MHz}$. Reaching the quantum limit with these oscillators corresponds to lowering the temperature to only a few millikelvin, which is not experimentally accessible with present day technology. To circumvent this problem, while still using conventional beam oscillators as that shown in Fig. 2.1, much scientific emphasis has recently focused on active cooling mechanisms. This is also the topic of two of the appended papers, the basic premises of which will be discussed in the following section.

2.3 Back-action cooling

A refrigerator works by removing heat from the interior and depositing it outside, thus lowering the temperature inside the refrigerator. In doing so it draws energy from an external source which is used to compress, expand and pump the refrigerant liquid used for heat absorption. The lowest temperature a refrigerator can achieve (the base temperature) is set by the refrigerant liquid as this controls the amount of energy absorbed. In this way, liquid helium dilution refrigerators are able to cool down to base temperatures of $\sim 25\,\mathrm{mK}$. To make things yet cooler is however a problem as the base temperature cannot be lowered indefinitely. Reaching the quantum limit of most mechanical oscillators is thus a challenge; a temperature of $T = 20\,\mathrm{mK}$ corresponds to $\omega = k_B T/\hbar \simeq 2.6\,\mathrm{GHz}$. Furthermore, any measurement on the oscillator will in practice always result in some heating, thus increasing the temperature of the oscillator further.[2]

To eliminate this problem scientists have to resort to active cooling mechanisms. In doing so one wishes to stimulate transitions in the system so that it loses energy at a rate which is faster than the rate at which it comes to thermal equilibrium (i.e. is heated to the temperature of the surrounding media). Here cooling refers to removing energy from a given subsystem of the bigger system so that its motion corresponds to an effective temperature which is lower than the thermal background. This type of cooling can be achieved in many ways, the most simple of which is active feedback cooling. In this method the motion of the object to be cooled is continuously monitored and analysed. Based on this information, the object is stimulated externally so that its motion is suppressed, thereby counteracting any forces which might perturb it. Using this technique, near to ground-state cooling of a macroscopic kilogram-scale oscillator was recently reported at the Laser Interferometer Gravitational Wave Observatory (LIGO) [13] (the reported level of cooling corresponds to an effective temperature of the mirror oscillator of $1.4\,\mu\mathrm{K}$ which equates to a

[2] As an example, O'Connell et al. [12] used a base temperature of 25 mK to reach the quantum limit although this should in theory be possible for much higher temperatures; $T \sim 0.3\,\mathrm{K}$ for the reported mechanical frequency.

population of the vibrational modes which is only a factor of 10 away from the ground state).

Active feedback cooling is however only applicable for low frequency oscillators (up to 1 kHz range). For oscillators with higher mechanical frequencies the method cannot be used with great accuracy as the mechanical motion of the oscillator is too fast. This implies that the electronic monitoring of the oscillator will often lag the actual motion, causing the drive pulse to be delayed. Active feedback cooling is thus not reliable for high frequency oscillators as it may lead to more, rather than less, energy being supplied to the subsystem to be cooled. To get around this problem, methods which do not rely on any electronic monitoring should be employed, which is often referred to as back-action cooling. Suggestions for different back-action cooling schemes come in many different forms, see for example Refs. [14–20]. Common to these is that the mechanical oscillator interacts with either an electromagnetic field, e.g. light, or a flow of charge carriers, e.g. an electrical current, in a way that it on average loses energy to the surrounding media. This is also the basic premises behind Papers III-IV as discussed further in Chapter 5.

One method which easily describes the concept of back-action cooling is cavity cooling as sketched in Fig. 2.3(a). In its simplest form, this method uses an optical cavity where one of the two high-finesse mirrors has been replaced by a mechanically compliant mirror, often in the form of a membrane.[3] Consider at first the situation when the oscillating mirror is not moving. Under such conditions the optical cavity will have a natural frequency ω_c at which incident laser light will form a resonant pattern known as a standing wave inside the cavity. Once one of the mirrors is replaced by a mechanically compliant mirror this resonance pattern will be changed due to the motion of the mirror. The effects of these changes on the system are two-fold:

i) Each time a photon is reflected it exerts a force on the mirror in accordance with Newton's third law of motion. The combined effect of all photons in the cavity is known as the radiation pressure force. Seeing that the position of the membrane affects the resonance conditions in the cavity, this implies that the average force on the membrane will depend on its position. The overall effect of the radiation pressure force on the membrane thus depends on the frequency of the input laser field ω_d which implies that the membrane may be either pumped or cooled. This is indicated in Fig. 2.3(b) where $\omega_d < \omega_c$ and the membrane is cooled (the area under the blue curve is larger than the area under the red curve).

ii) Much like the example of active feedback cooling discussed above there is also a delay-effect in the optical cavity. This comes about as the number

[3] An optical cavity consists of two parallel high-quality mirrors which bounce light back and forth many times. For a cavity of a given length, only light at certain frequencies will achieve resonant conditions to produce standing waves in the cavity.

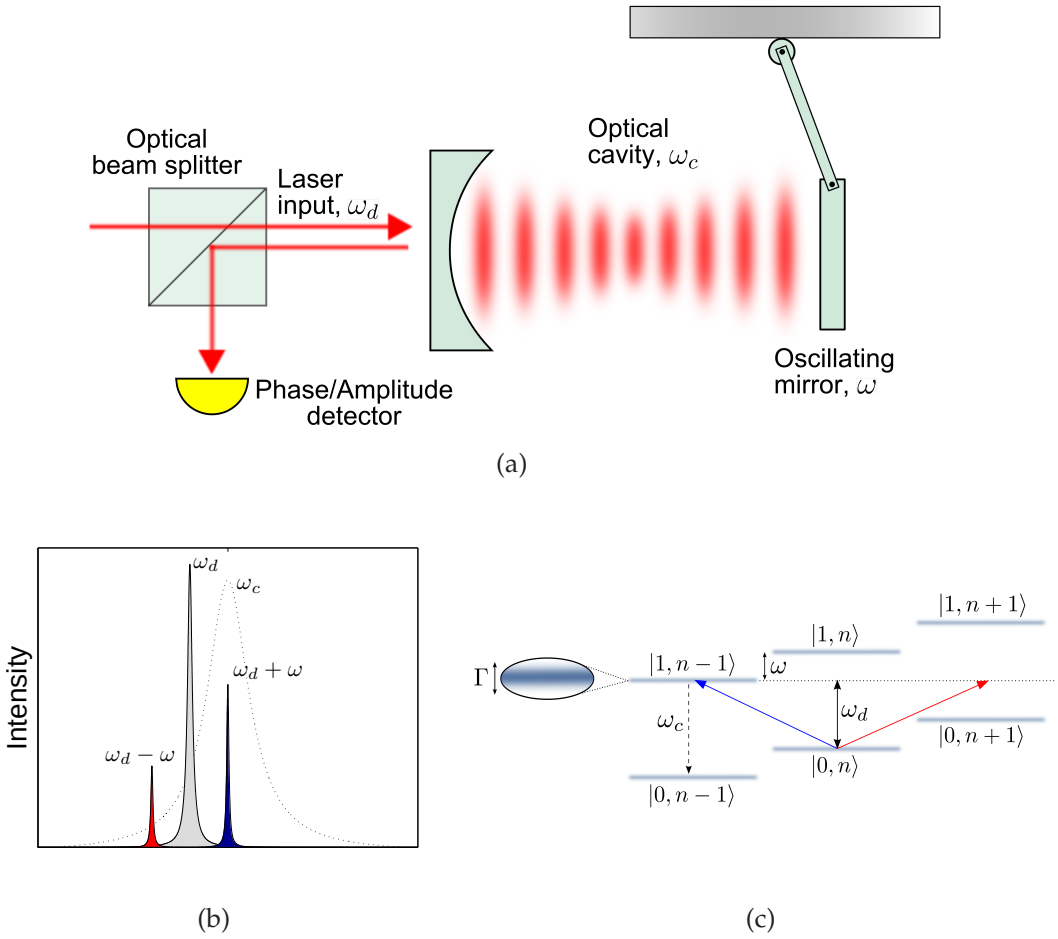

Figure 2.3: (a) Schematic diagram of an optical cavity with an oscillating mirror. The mechanical motion of the mirror changes the resonant conditions in the cavity, which modulates the phase and the amplitude of the laser field depending on the mirror's position. By analysing the detected laser light the motion of the oscillator can be inferred. (b) By tuning the incident laser light to one of the optical sidebands, pumping or cooling of the mechanical oscillator is possible. Here, the input laser frequency is $\omega_d = \omega_c - \omega$, under which conditions the oscillator loses energy to the optical cavity (blue cooling peak is larger than red heating peak). (c) Corresponding energy level diagram in the resolved sideband limit. Here, the optical cavity is considered as a two-state system $(0, 1)$ and the movable mirror is modelled as a quantum oscillator with energy quanta labelled by n. In the above, the cooling channel $|0, n\rangle \rightarrow |1, n-1\rangle$ is associated with the operator $\hat{b}$ which lowers the state of the oscillator. The decay $|1, n-1\rangle \rightarrow |0, n-1\rangle$ corresponds to the emission of an optical photon of frequency ω_c into the cavity. Transitions through the heating channel (associated with the operator $\hat{b}^\dagger$) are here suppressed due to the limited broadening of the energy levels, $\omega > \Gamma$.

of photons in the cavity does not immediately equilibrate to the position of the membrane.

As both surfaces in the cavity are highly reflective mirrors, the optical finesse $\mathcal{F}$ is high and the optical linewidth Γ is narrow.[4] This implies that the photons leak out of the cavity slowly such that changes in the position of the membrane are not immediately reflected in the number of photons in the cavity. This is the cause of the aforementioned cavity delay, which in the case of red-detuning ($\omega_d < \omega_c$) may cause the resonator to lose energy to the cavity.

The combination of these effects may cool the membrane depending on the frequency of the input laser. The efficiency of the cooling depends both on the power of the input laser, the optomechanical coupling as well as on the optical linewidth Γ as discussed below, see also Refs. [21–24].

2.3.1 Reaching the ground state

In order to reach the quantum mechanical ground state of an oscillator as that shown in Fig. 2.3(a) it is not only sufficient to promote cooling over heating processes as discussed above. One must also ensure that the rate of cooling is by far the fastest thermal transport rate in the system in order for the oscillator to be sufficiently insulated from both the thermal environment and transitions involving an increase in the number of mechanical energy quanta. The former of these constraints corresponds to having a large mechanical quality factor $Q \gg 1$ (low thermal damping), which is often not a problem in optical cavities. Satisfying the latter condition corresponds to reaching the so-called resolved sideband limit, $\omega > \Gamma$.

The underlying mechanics of this is sketched out in Fig. 2.3(c). Here, the optical cavity is considered as a two-state system; any interaction with the movable mirror will change the state of the cavity through the associated absorption/emission of photons by the oscillator. In other words, due to the motion of the mirror an incoming photon at frequency ω_d may be reflected as a photon at the cavity frequency $\omega_c = \omega_d + \omega$ if it absorbs the corresponding amount of energy from the mechanical oscillator. If this happens, the total energy of the oscillator is reduced by the amount $\hbar\omega$, and its energy (and thus motion) corresponds to a temperature which is lower than the thermal background, see equation (2.3).

As the coupling between the laser field in the cavity and the position of the mirror is associated with the mechanical deflection operator $\hat{x} = x_0(\hat{b}+\hat{b}^\dagger)$, any

[4] The optical finesse $\mathcal{F}$ is a measure of the quality of a mirror, i.e. how much it reflects. The optical linewidth Γ gives a measure of how sharp the resonance in the cavity is. The optical finesse and the cavity linewidth are thus the optical analogues of the mechanical quality factor Q and damping γ discussed later.

interaction which changes the cavity from the state 0 to the state 1 will necessarily either increase or decrease the number of mechanical energy quanta n in the system. In order to reach the quantum mechanical ground state of the oscillator, it is thus necessary to ensure that the transitions which are associated with $\hat{b}$ (absorption of mechanical energy by the cavity) are greatly enhanced compared to the process associated with $\hat{b}^\dagger$ (wherein the oscillator absorbs energy from the cavity). This is accomplished by operating the input laser at the lower sideband $\omega_d = \omega_c - \omega$ in the so-called resolved sideband limit as shown Fig. 2.3(c). Under such conditions, the allowed energy levels for the cavity photons are narrow and transitions through the heating channel (red arrow) are greatly suppressed as there are no available states at the corresponding energy. At the same time, the laser drive is resonant with the cooling channel (blue arrow) which will be the dominant mechanism for energy transport in the system. Achieving these conditions, the average number of mechanical energy quanta can theoretically be cooled down to,

$$\langle n \rangle \sim \frac{\Gamma^2}{16\omega^2 + \Gamma^2} \ll 1\,, \qquad \omega > \Gamma\,, \tag{2.5}$$

which corresponds to reaching the quantum limit.

Presently, cooling of mechanical oscillators is a very active research topic both experimentally and theoretically. Around the world, several research groups are working hard to optimise their experimental setups to achieve this holy grail of quantum nanoelectromechanics. Recent reports suggest that this should by no means be impossible. For example, experimental realisation of the resolved sideband limit has been reported [21], although complete ground-state cooling using active cooling is yet to be realised, primarily due to limitations in the input laser power.

In Papers III-IV two different mechanisms to achieve this kind of cooling in suspended nanowire structures is discussed. The underlying theory of these papers is similar to the material discussed in the present chapter, with the main difference that we consider interactions between the mechanical motion and charge carriers rather than optical photons. The suggested mechanisms, although experimentally challenging in their own, thus avoid the complication of incorporating optical fields into dilution refrigerators. Also, optical cavities are less suited when working with nanowires as the optomechanical coupling scales with the cross-sectional area available to the photon field.

2.3.2 Quantum limited measurements

What new phenomena do we expect to observe if we manage to put a system like the suspended nanowire structures discussed in this thesis into their quantum mechanical ground state?

First of all, any quantum system will be very sensitive to external perturbations. This implies that even the slightest change in the mass of the object or the forces on it will be enough to change the quantum state of the system. Thus, a sufficiently cooled suspended nanowire or membrane in an optical cavity will in principle have a sensitivity where the extra weight of one atom or a minute change in the displacement of the oscillator will be enough to change its quantum state. A further challenge is to ensure that also the detection mechanism which couples to the mechanical element is sensitive enough to register these quantum transitions. In the field of quantum nanoelectromechanics, detection and transduction are equally important as the possibility to prepare the mechanical system in its motional ground state. Achieving only one without the other means that you gain nothing as you will not be able to verify and detect your system. Over the last decade there have been an increasing number of reports on detection at or close to the quantum limit, see e.g. Refs. [17, 25–28].

Secondly, achieving the quantum limit means that one can couple the mechanical system to some other quantum system, e.g. a quantum dot. In this way, the mechanical system can be used to transmit information on the quantum state of the dot to an electronic readout with minimal losses. These kinds of systems have been proposed as model setups for hybrid quantum information applications.

Finally, the possibility to put an object like a suspended nanowire in its motional ground state opens up the possibility to observe exotic phenomena (superposition, entanglement etc.) in macroscopic samples. Achieving this means that one could for example probe if the oscillator is in two places at once, which is the underlying principle behind quantum superposition. Thus, reaching the quantum limit will allow for quantum experiments on objects that we can see and manipulate under a microscope, something which is hardly possible with objects that we normally consider to behave quantum mechanically, i.e. atoms. Achieving the quantum limit in nanoelectromechanical systems will thus test our understanding of quantum theory at a scale not previously accessible.

For a more detailed discussion on the possibilities presented by reaching the quantum limit the reader is referred to the focus issue of New Journal of Physics and references therein [29].

Acknowledgement
The graphical illustrations in this chapter have been inspired by work from Tobias Kippenberg and Kerry Vahala [22] and the PhD thesis of Meno Poot [24]. All work presented is by the author unless otherwise stated.

CHAPTER 3
Superconductivity

In 1962 Brian D. Josephson discovered what was later to be called the Josephson effect [30]. In this chapter I briefly discuss this effect, as well as some properties of the superconducting state. The chapter also introduces Andreev reflection and Andreev bound states, concepts which are important for the following discussion.

3.1 The Josephson effect

The Josephson effect is the name given to the physical phenomenon of a current flow across two superconductors separated by a thin insulating layer (see Fig. 3.1). In particular the theory predicts that if no battery connects the two superconducting leads (the voltage bias is zero), a finite direct current will nevertheless flow between them. Applying instead a steady bias voltage V, the resulting current over the junction will oscillate with the frequency $2eV/\hbar$. These results are very counter-intuitive. Normally, we would expect no current through a junction if we supply no power, i.e. no battery is connected. Similarly, if we apply power through a battery which delivers a constant amount of energy per unit time to the junction we expect the current through it to be constant.

The origin of the Josephson effect derives from the general physical properties of superconductors. If one performs an experiment where one measures the resistivity of a metal as a function of its temperature one expects to see the former go down as the temperature is reduced. This is a well-known physical result which derives from the fact that the atoms in the metal vibrate less as you lower the temperature, thus reducing the amount of electronic scattering and promoting charge transport. However, for some metals one finds that the resistivity abruptly falls to zero at temperatures below approximately 1 K. Below this temperature, called the critical temperature, the metal is said to be superconducting as it can sustain electrical currents without any losses.

To understand these effects one has to enter the world of quantum mechanics as superconductivity is intrinsically a quantum phenomenon. In short, the superconducting state can be characterised by spatially separated electrons forming bound pairs which condense into a single quantum state which

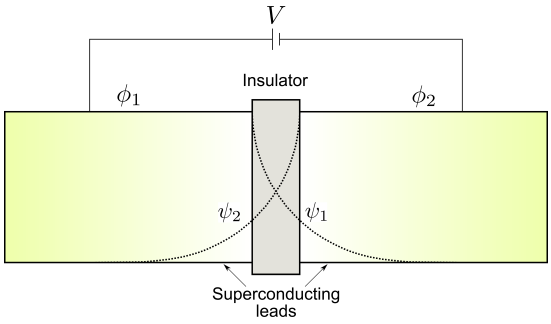

Figure 3.1: Schematic diagram of a Josephson junction. Two superconducting leads are connected by an insulator. If the insulating region is short (compared to the superconducting coherence length), the wave function for the electronic state in the lead (ψ_1 and ψ_2 respectively) can tunnel through the insulating region and overlap with the wave function in the opposite lead. This creates an interference phenomenon between the wave functions, the outcome of which is a flow of charge particles through the insulating region (see equation (3.1)). Applying a bias voltage V over the junction, the phase difference $\phi = \phi_2 - \phi_1$ varies linearly in time and the current over the junction oscillates at the frequency $2eV/\hbar$.

dictates the properties of the superconductor. In other words, two electrons, which may be far apart, have linked together to form what is known as a Cooper pair [31]. What holds the electrons in the Cooper pair together is a very weak attractive force which derives from the vibrations of the atoms in the metal. Due to the limited strength of this force, only a slight increase in temperature (increased relative motion of the atoms in the metallic lattice) is sufficient to break up the pair. This explains why superconductivity is only seen at low temperatures.

Once a metal turns superconducting, the majority of the electrons in the system will combine in Cooper pairs. These new "particles" behave differently from the normal electrons. In particular, the Cooper pairs all collapse into a single quantum state called the condensate which is protected from other (dissipative) states by an energy known as the superconducting gap (see Section 3.2). The superconducting state is thus characterised by a pairing between the electrons in the sample into Cooper pairs, which can all be described through a common wave function associated with the condensate.[1]

To formalise this one can describe the state of the electron pairs in the condensate through a macroscopic wave function with a phase ϕ common to all Cooper pairs in the sample. What Josephson showed was that if two superconducting metals are separated by a thin insulating barrier, Cooper pairs can tunnel between the two superconducting regions. Furthermore, the overlap

[1] In a normal metal the opposite is true, i.e. two electrons cannot be found in the same quantum state due to a quantum mechanical exclusion principle known as the Pauli principle.

of the wave functions in the leads (see Fig. 3.1) will correlate the evolution of their respective phases, which will in turn depend on the voltage bias over the junction. This is the Josephson effect which is normally described through the equations (for a detailed derivation see e.g. Refs. [32–34]),

$$I = I_c \sin(\phi + \phi_0) \,, \tag{3.1a}$$

$$\frac{\partial \phi}{\partial t} = \frac{2eV}{\hbar} \,. \tag{3.1b}$$

Here, the current I through the junction is proportional to the sine of the phase-difference ϕ between the two superconductors with ϕ_0 a constant phase offset. The phase-difference ϕ is in turn related to the applied bias voltage V according to equation (3.1b). These equations are the central result of Josephson's analysis. As can be seen, they predict a non-zero dc current at zero bias voltage due to the phase difference ϕ_0, such that a maximum current of I_c (the critical current) can flow through the junction with zero potential drop. Similarly, a finite bias voltage V will continuously change the phase-difference, resulting in a current which oscillates in time at a frequency $2eV/\hbar$.

3.2 BCS theory

Having outlined the basic mechanism behind the Josephson effect, the following section will briefly discuss the BCS theory of superconductivity. This theory was introduced in 1957 by Bardeen, Cooper and Schrieffer in order to explain many of the peculiar phenomena observed in superconductors [35,36]. In short, the BCS theory explains how an attractive potential, however weak, is sufficient to form bound electron pairs in a metal at low temperatures.

To describe the formation of a Cooper pair one can think of an electron in the metal which is interacting with the positively charged atoms in the lattice. As the electron is negatively charged it will attract nearby positive charges, thus creating a deformation in the atomic lattice. This deformation will be felt by the other electrons in the sample. In particular, the BCS theory predicts that the deformation of the atomic lattice will cause a second electron (with opposite spin) to move into a region with higher positive charge density such that the two electrons become correlated. Under these conditions, the two electrons form a pair which is held together by the motion of the atoms in the lattice. Pairs like this will be formed by many of the electrons in the sample creating a large number of Cooper pairs which interact amongst each other (due to distortions in the lattice). The outcome of this is that the electron pairs can be described as a collective state, the condensate, due to their correlated motion.

If one were to break up one electron pair, one necessarily also change all other pairs in the sample as the overall electron-lattice interaction would

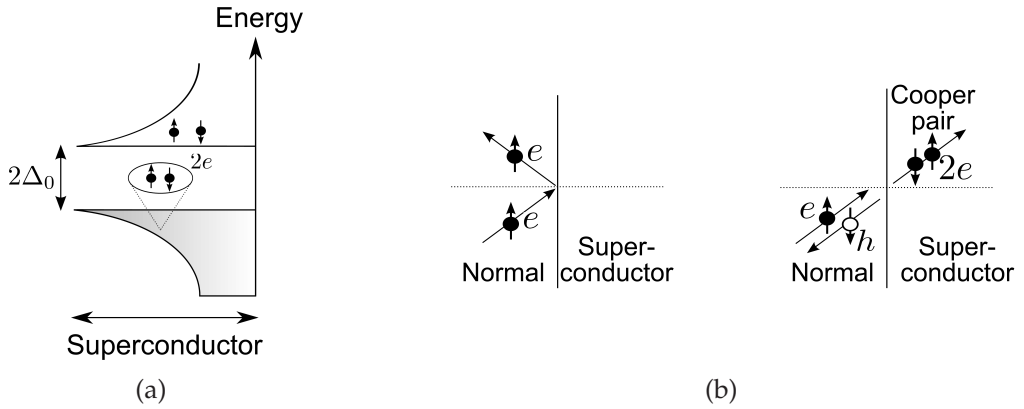

Figure 3.2: (a) The superconducting state. The superconductive condensate (shaded region) is formed by the Cooper pairs $(2e)$ in the system. The condensate is separated from the continuum by the energy gap $2\Delta_0$, which means that a minimum of this energy is required to create two electronic (e) excitations by breaking up a Cooper pair. (b) Normal (left) and Andreev (right) reflection between a normal metal and a superconductor. In normal reflection the electron is reflected as an electron, whereas Andreev reflection converts the electron to a hole (h) in the normal metal, thereby avoiding forbidden single-particle transmission within the superconducting gap. To uphold charge conservation, Andreev reflection is associated with the creation of a Cooper pair in the superconducting condensate.

change. If the energy needed for this to happen is smaller than the energy provided by the motion of the atoms in the lattice, the Cooper pairs will not be sensitive to this motion and the resistivity will be zero.[2] This is the case at low temperature where the lattice phonons (collective motion of the atoms) are not very energetic.

In order to break up a Cooper pair one thus has to change not only the pair to be dissolved, but also all other pairs in the sample. This requires an amount of energy which is substantially larger than the energy required to dissolve just the one pair. Often one speaks of an "energy gap" for the creation of single-particle electrons from the superconducting condensate. This gap gives a measure on the minimum energy required to create two normal, dissipative electrons in the sample. This is shown pictorially in Fig. 3.2(a) where the superconducting condensate is indicated by the lower shaded regions. To create an excitation (free conducting electrons) in the metal, an amount of energy $2\Delta_0$ is required in order to break up one Cooper pair. Here, Δ_0 is often referred to as the superconducting gap (energy separation from the chemical potential). In a homogeneous superconductor no electronic quantum state are available

[2]Resistivity can be thought of as a measure of how much lattice vibrations influence the motion of the electrons in the sample. If these vibrations are not sufficient to break up the Cooper pairs, these will be unaffected by the motion of the atoms and the Cooper pairs can conduct electric current without any losses.

inside the superconducting gap as shown in Fig. 3.2(a).

Not all electrons in the sample will be found as pairs in the superconducting condensate, some will remain unpaired at finite temperature. These electrons can be thought of as excitations from the superconducting condensate, i.e. they are found in the region above the superconductive gap in Fig. 3.2(a) which can accommodate free electron states. The proportion of such electrons depends on the external temperature as this controls the energy of the lattice vibrations and thus the number of formed Cooper pairs. Alternatively, this can be interpreted as the superconductive gap being temperature-dependent, i.e. it goes to zero at the critical temperature, in which instance the superconductive state disappears.

3.3 Andreev reflection

Next I discuss what happens if a region of normal metal, rather than an insulator, is sandwiched between the two superconducting leads. This is the scenario considered in Papers II-IV, where the normal metal region is substituted by a suspended metallic nanowire.

Unlike insulators, metals conduct electricity very well since the conduction electrons are only loosely bound to the atoms in the material. As such, the metallic region can sustain electrons which are free to move through the sample. When electrons in a normal metal (N) region impinge on a boundary to a superconducting (S) region they can be reflected back into the metallic body either as electrons or holes. The latter of these two mechanisms, known as Andreev reflection after A. F. Andreev who first analysed the phenomenon [37], is unique to superconductor - normal metal junctions, the origins of which will be discussed below. Note that Andreev reflection is not seen at the boundary between an insulator and a superconductor region as no free electrons are found in the former.

In order to explain Andreev reflection we consider the interface between a normal metal and a superconductor, an N-S boundary. In his work, Andreev showed that an electron impinging from the normal metal with an energy E which is inside the superconducting energy gap Δ_0 in the superconductor can be reflected back into the normal metal as a hole.[3] Ordinarily, one would only expect the electron to be reflected as an electron. However, through the process introduced by Andreev, the electron-like excitation could alternatively be reflected as a hole-like excitation with the same energy E but opposite momentum (see e.g. Ref. [38]). This comes about as there are no available electronic states in the superconductor for energies $|E| < \Delta_0$. The electron will

[3] A hole is not a real particle but rather an electron vacancy. As an analogy, a hole can be thought of as the little air bubble left if one were to be able to remove a drop of water from the bottom of a jar otherwise full of water.

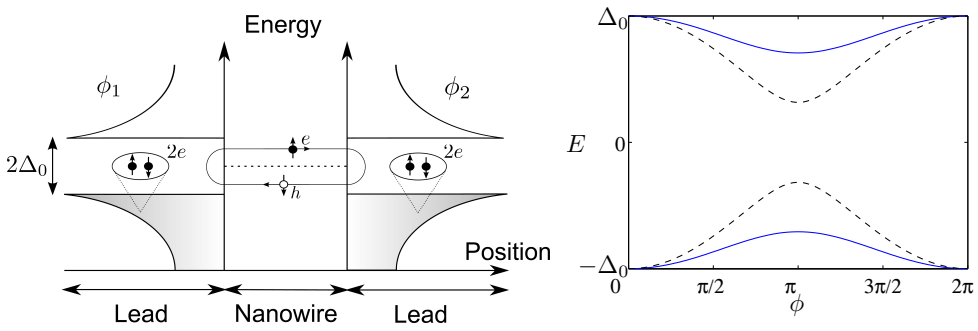

Figure 3.3: Andreev bound states. (a) Two superconducting leads are connected by a normal metal region. An electron (e) in the normal metal impinging on the right superconductor is Andreev reflected back into the normal metal as a hole (h). Due to conservation of charge, this process is associated with the creation of a second electron in the right superconductor and a Cooper pair ($2e$) is formed. At the left interface, the hole is reflected into the normal metal as an electron, a process which involves the destruction of a Cooper pair in the left lead. In this way, charge is transferred through the junction at a rate which depends on the phase difference $\phi = \phi_2 - \phi_1$. (b) Energy dependence of the Andreev bound states, equation (3.2), shown for two junction transparencies D_1 (solid) and D_2 (dashed) where $D_2 > D_1$.

thus not be able to pass into the superconductor. If however, the electron can be reflected as a hole, charge conservation implies that the process has to be accompanied by the transfer of two electrons into the superconducting region. The two transferred electrons now form a Cooper pair which can readily join the quasiparticle continuum in the superconductor. A schematic diagram of normal and Andreev reflection is shown in Fig. 3.2(b).

3.3.1 Andreev bound states

Consider now an S-N-S junction. In this situation Andreev reflection can occur at both interfaces i.e. the reflected hole at the right interface gets reflected into an electron at the left interface (the opposite process is also present which accounts for the formation of two Andreev states). As these processes are elastic (energy conserving) the reflected particles can interfere and form bound electronic states in the junction as shown in Fig. 3.3(a). The energy dependence of these bound states is found by matching the wave functions in the different regions [39–41]. The resulting bound states split into two Andreev levels, one above and one below the chemical potential, with their phase-dependent energies given by,

$$E_{\pm} = \pm\Delta_0\sqrt{1 - D\sin^2(\phi/2)}\,. \tag{3.2}$$

Here, ϕ is again the superconducting phase-difference and D is the normal state transparency. In the above, the branch E_+ is composed of electrons and holes travelling in opposite longitudinal direction of the junction. By symmetry the branch E_- has the opposite composition.

A plot of these bound Andreev states as a function of the phase-difference is shown in Fig. 3.3(b). Considering that electrons and holes are charged particles one can conclude that the Andreev states carry current through the junction. This can again be understood by considering the simple example of a right moving electron in the normal region. As it is Andreev reflected at the right superconductor a left moving hole (opposite charge) is created in the normal region. For bound states these reflected paths interfere hence each instance of reflection transmits charged particle through the junction. The current carried by a populated Andreev state is given by,

$$I(\phi) = \frac{2e}{\hbar}\frac{\partial E(\phi)}{\partial \phi}\,. \tag{3.3}$$

The Josephson relation for the current (3.1a) is recovered from the above in the limit of low junction transparency $D \ll 1$ which is the condition originally considered by Josephson. The critical current in this limit is $I_c = e\Delta_0 D/(2\hbar)$.

In Papers II-IV the normal metal region of the S-N-S junction is replaced by a short suspended nanowire in the form of a carbon nanotube. Normally, carbon nanotubes are not superconducting. If however a short ($L \lesssim 1\ \mu$m) tube connects two superconductors, coherent charge transport through the junction is possible and the superconductors become correlated. These phenomena have been studied experimentally by several groups (see e.g. Refs. [42–46]) and it was recently shown that bound Andreev states are indeed formed in these types of junctions [47,48]. This is discussed further in Papers III, where a transverse magnetic field is used to couple the current carried by the electronic Andreev states to the mechanical motion of the suspended nanowire.

CHAPTER 4
Carbon nanotubes

As discussed in previous chapters, nanoelectromechanical systems are based on mechanical oscillators which can trigger an electronic or mechanical response to external stimuli. Such oscillators come in different forms and shapes with various pros and cons attributed to them. For example, metallic or semiconducting beam oscillators are often used in nanoelectromechanical systems. These typically have high mechanical frequencies and high quality factors, which would make them ideal for sensing applications. However, due to the relatively large mass their zero-point amplitude is small, which means that the electromechanical coupling in these systems is typically not very good.

Ultimately, the goal of nanoelectromechanical systems is to use them for quantum limited sensing applications. To achieve this, the systems must not only have a high enough mechanical frequency in order for it to be possible to cooled them to the quantum regime. Equally important is that sufficiently strong electromechanical coupling can be achieved in order to detect and analyse changes to the system. A very promising candidate for this is carbon nanotube-based systems as these combine high mechanical frequencies with a large zero-point amplitude making them, in principle, ideal for practical applications.

4.1 A cylinder of carbon

Carbon nanotubes are hollow cylinders of carbon atoms with diameters on the nanometre-scale. These can be either single-walled or multi-walled (many tubes inside one another) and have varying electronic properties depending on their wrapping. Furthermore, carbon nanotubes are one of the strongest materials known to man with Young's moduli in the TPa range [49, 50], making them 100 times stronger than steel while being six times as light. To put this into perspective; it has been calculated that a chain of carbon nanotubes would be sufficiently strong to be used as a self-supporting lift to the moon.

Carbon nanotubes have since the early 1990's been heralded as one of the most exciting materials for novel nanotechnological applications, primarily due to their small size and unique one-dimensional electronic properties. To date, real applications are however few. One notable exception is perhaps

recently developed bolometers which use forests of vertically aligned carbon nanotube as nearly perfect absorbers of light [51]. Other proposed carbon nanotube based applications which have yet to reach the market include conductive papers and textiles [52, 53], adhesives which behave like the feet of a gecko [54], high-capacity lithium ion batteries [55] and high impact bullet-proof vests [56]. Focusing instead on applications where the characteristics of the individual tubes are of importance (which are much harder to manufacture) even more exotic devices can be found in the literature. For example, suspended carbon nanotubes have been made to operator like nanoscale motors which can shuttle cargoes back and forth along their length [57, 58] or be used as linear bearings [59]. Also, a nanotube radio based on a single carbon nanotube cantilever has been reported [60].

Carbon nanotubes thus offer great potential both for macroscopic and microscopic applications. The big challenge in realising their potential lies in the growth of the tubes. To date, proposed devices which are envisaged to reach the market do not utilise the full potential offered by carbon nanotubes. The reason for this is that their growth cannot yet be controlled to satisfy predefined properties. Once this level of control can be achieved, of which tentative progress has recently been made [61, 62], applications utilising the full potential of carbon nanotubes, e.g. single molecule components for electronics applications, could see the light of day.

The present thesis focuses on electronic transport through suspended, vibrating nanowires and the effects of electromechanical interactions in these systems. Below a brief discussion of some characteristic properties of carbon nanotubes important for this thesis are discussed. For a more detailed discussion the reader is referred one of the many reviews on carbon nanotubes available in the literature.

4.1.1 Mechanics of suspended carbon nanotubes

What makes carbon nanotubes ideal nanomechanical oscillators is not only that they are very stiff, but also that they are hollow. This implies that they are many times lighter than their solid counter-parts. Considering that both the mechanical frequency ω and the zero-point amplitude x_0 scale inversely with the mass, this implies high resonance frequencies and comparatively large zero-point amplitudes. The fact that the carbon nanotubes are hollow also implies that although they are very stiff in the longitudinal direction they are quite susceptible to deformations perpendicular to their axis. For example, a suspended carbon nanotube can easily be made to oscillate if a periodic force is applied to it, see Fig. 2.1.

Another important property for nanoelectromechanical applications is that the mechanical subsystem does not dissipate energy too quickly and that it is sensitive to external perturbations. Both these properties are related to the

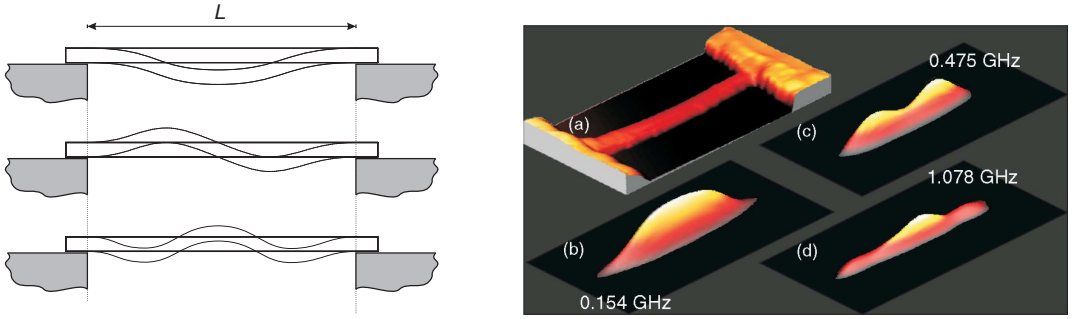

(a) (b)

Figure 4.1: Vibrational profile of a suspended beam oscillator. (a) The theoretical profile of the three lowest modes of vibration of a doubly clamped suspend beam of length L. (b) The equivalent experimental plot for a 770 nm suspended carbon nanotube. The first image shows the profile of the stationary tube whereas the profile of the 3 lowest vibrational modes with the corresponding measured frequency $f_i = \omega_i/(2\pi)$ is shown in image two-four. The images were obtained by an atomic force microscope in close proximity above the resonating nanotube. Adapted from Ref. [65].

mechanical quality factor Q, which is a measurement of the resonance profile of the system. Until recently, low mechanical quality factor was one of the biggest problem facing carbon nanotube-based nanoelectromechanical systems. As an example, the reported mechanical quality factor in the seminal paper by Sazonova *et al.* [63] was only $Q \sim 100$, which made the device very limited. Seeing that carbon nanotubes are (at least in theory) impurity free, all-carbon structures with a very well-ordered atomic composition these low quality factors was for a long time seen as somewhat mysterious as they did not correspond to the theoretical predictions. This matter was however recently resolved, primarily through changes in the growth mechanism of the tubes, with quality factors as high as 10^5 being reported [64]. With these improvements in fabrication technology, carbon nanotube oscillators are finally at the stage where the systems can be manufactured to such high standards that they can be used to probe the quantum limit.

As mentioned earlier a suspended carbon nanotube can in many respects be thought of as a beam free to vibrate between its clamping points. This is of course a crude generalisation as the motion of the tube is ultimately governed by the motion of the atoms from which it is constructed. Seeing that a carbon nanotube is a hollow cylinder typically only a few hundred nanometres long it is reasonable to question whether it is viable to describe it in the above language of a continuous solid beam rather than from an individual atomistic perspective. For the flexural (bending) vibrations considered here however, numerical results based on the motion of the individual atoms is comparable

to the results from a continuum analysis where the nanotube is considered as a mechanical beam with known physical properties. The difference between these methods of analysis is of course that the atomistic perspective not only gives the frequencies of the bending modes of the tube but also the other so-called phonon branches, i.e. radial breathing mode (RBM), longitudinal (stretching) mode etc. These are however not considered in this thesis.

We may thus describe the bending motion of a suspended carbon nanotube in the language of continuum mechanics with the frequency of the resonance modes given by,

$$\omega_i = k_i^2 \sqrt{\frac{EI}{\rho S}}\,. \tag{4.1}$$

Here, E is the Young's modulus, I is the area moment of inertia which depends on the tube radius, ρ is the mass density of the tube and S is the area. In equation (4.1), ω_i is the resonance frequency where $i = 1, 2, 3, ...$ labels the resonance mode. Finally, the coefficients k_i are inversely proportional to the length of the tube and are determined from the boundary conditions of the doubly-clamped beam. For a carbon nanotube the mechanical frequency is typically very high ($\omega_1 \sim$1 GHz) due to the high mechanical stiffness (E), low mass (ρ) and small area (S). In Fig. 4.1(a) a schematic diagram of the three lowest modes of vibration is shown. Similarly, Fig. 4.1(b) shows an experimental visualisation of these three modes for a suspended carbon nanotube.

Experimentally, the mechanical frequencies of carbon nanotubes are typically lower than the theoretical predictions (4.1), which makes reaching the quantum limit challenging. The reason for this is unclear, but is probably related to impurities which attach to the tubes during the fabrication process. If instead the higher resonance modes are considered, greater mechanical frequencies can be realised (see Fig. 4.1(b)) at the cost of a lower zero-point amplitude $x_0 \propto \omega^{-1/2}$ and thus weaker electromechanical coupling. Also other phonon branches, which have much higher mechanical frequencies, can and have been used [66]. These are however, typically much harder to access and manipulate experimentally. In the present thesis only the lowest, fundamental, bending mode is considered.

4.1.2 Electronic properties of carbon nanotubes

To conclude a short discussion about the electronic properties, which are perhaps even more spectacular than the mechanical properties, of carbon nanotubes is presented. Since the focus of the appended papers is the electromechanical interactions in the systems only the most important aspects will be mentioned. For a more thorough discussion the reader is referred to one of the many review articles on the subject, e.g. Refs. [67, 68].

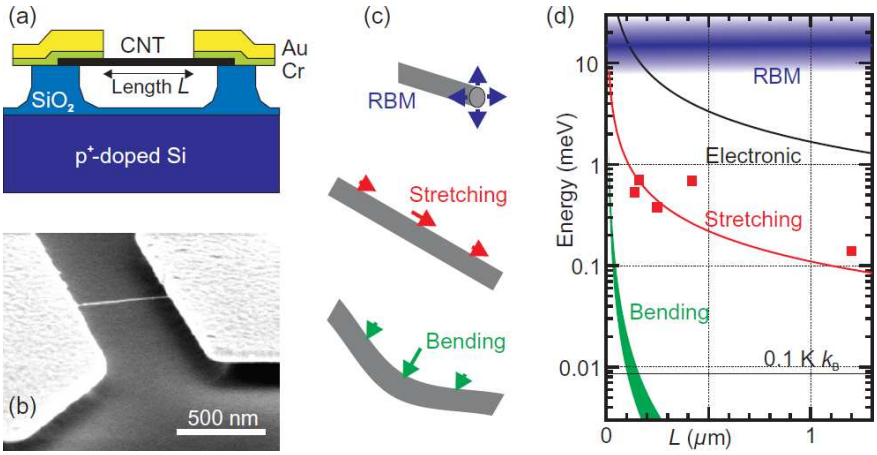

Figure 4.2: Phonon modes of a suspended carbon nanotube. (a) Schematic diagram of a typical gated suspended carbon nanotube (CNT) structure. (b) Scanning electron micrograph of the corresponding system. (c) Schematic diagram of 3 different families of phonon modes in the nanotube. In this thesis only the low-energy bending modes is considered. (d) Theoretical (lines) and experimental (squares) energy of oscillation as a function of the nanotube length (E =0.01 meV is equivalent to a frequency ω ∼15 GHz). The dashed horizontal line indicates the equivalent temperature of 0.1 K. All images adapted from Ref. [66].

As mentioned above, a carbon nanotube is in principle an all-carbon cylindrical structure with a regular atomic configuration. To understand its electronic structure one has to take one step back and consider graphene, which is the 2-dimensional equivalent of the virtually 1-dimensional carbon nanotube. Without going into too much detail, graphene is a zero bandgap semiconductor or a semi-metal. In other words, graphene is just about a semiconductor in that it has a valence and a conduction band separated by a bandgap.[1] The special thing about graphene is however that the bandgap is zero; the material is at the same time almost a metal. Furthermore, the electronic dispersion relation in graphene is linear close to the Fermi point, which implies that low-energy electrons in graphene behave just like relativistic particles with zero effective mass. These properties make graphene very unique in that it is a stable, truly 2-dimensional material whose electronic properties differ very much from those of normal 3-dimensional objects.

A carbon nanotube can be thought of as a rolled up cylinder of graphene. Indeed, many of the electronic properties that make grapheme so special also hold true for carbon nanotubes. However, there are also differences between the two carbon allotropes. The most striking of these is that the electronic

[1]The bandgap is the amount of energy one has to supply to an electron in a semiconductor to lift if the non-conducting valence band to the conduction band where the electron is free to move through the material

properties of a carbon nanotube depend on the way it is wrapped, i.e. how the underlying hexagonal lattice of carbon atoms which forms graphene is put together. When a sheet of graphene is rolled up to form a carbon nanotube the allowed electronic wave functions must be periodic in the circumference of the tube. This condition quantises the allowed electronic levels on the tube and the underlying graphene band structure splits into a series of 1-dimensional sub-bands. The outcome of this is that the tubes are either semiconducting (with a bandgap that depends on the diameter of the tube) or metallic (without a bandgap). Much of the research into nanotube growth has over the last decade focused on exactly this aspect; how to control the production of only metallic or semiconducting tubes of a given chirality (wrapping). To date little progress has been made from the perspective of actual growth, however post-production treatment has recently been shown to efficiently separate semiconducting from metallic tubes [61, 62].

For the material presented in this thesis, only metallic carbon nanotubes are considered. Seeing that these are virtually 1-dimensional conductors, electronic reflection is greatly suppressed due to the confined geometry. This implies that an electron in a clean carbon nanotube can travel coherently over distances up to a few microns without being scattered (ballistic transport), thus making metallic carbon nanotubes very good conductors at the same time as being mechanical oscillators of very high quality [69].

CHAPTER 5

Summary of the appended papers

In this chapter a summary of the appended papers is presented. Extensive information about the motivation, calculations, physical parameters, results and analysis of the results is found in the publications whereas this chapter serves to give an overview and complement to these. Below I present some of the most interesting results from the publications and try to motivate these in terms of the underlying physical processes. For a more detailed analysis the interested reader is referred to the appended papers and the appendices of this thesis where additional analytical results are presented (see also Refs. [70,71]).

5.1 Paper I - Electromechanically induced current deficit

In Paper I we analyse how the coupling between the motion of the nanowire and the flow of electrons through it affects the charge transport through the voltage-biased suspended nanowire junction depicted in Fig. 5.1. From this analysis we find that the magnitude of the magnetic flux Φ swept out by the vibrating nanowire controls the number of allowed electronic tunnelling channels. This effect is shown to result in a suppression of the flow of electrons at low temperatures, in which case the current through the junction is reduced by a factor $\propto \Phi^2$ compared to the case of no magnetic field.[1]

5.1.1 System and electromechanical coupling

Fig. 5.1 shows a schematic diagram of the system considered in Paper I where a suspended nanowire of length L is free to oscillate in the transverse magnetic field H. Expanding on the original work of Shekhter et al. [78], we analyse the system under conditions of strong spatial quantisation of the electronic energy levels on the nanowire and evaluate the flow of electrons over the junction in the presence of the magnetic field. Here, the significance of the energy level

[1] Electronic transport coupled to the vibrational motion of single molecules or quantum dots like the system under consideration has been a very active field of research over the decade, see e.g. Refs. [72–77].

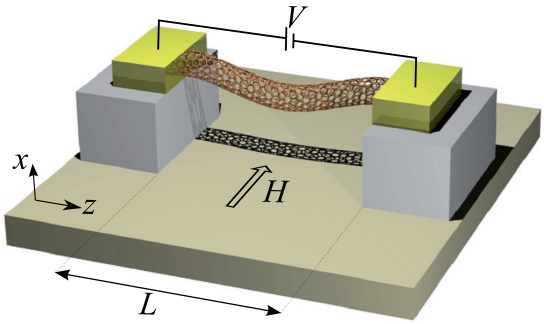

Figure 5.1: Schematic diagram of the system discussed in the appended papers. A nanowire of length L is suspended over two leads (normal metal or superconducting). By either voltage- or current-biasing the junction we analyse the system when the mechanical degrees of freedom (vibrations of the nanowire) are coupled to the electronic degrees of freedom (flow of charge carriers between the leads) by the transverse magnetic field H.

quantisation is that it implies that no real electronic states on the nanowire are allowed if the bias voltage is smaller than the energy level spacing $\Delta E \simeq \hbar v_F/2L \sim 0.25\,\text{meV}$ where v_F is the Fermi velocity. Under such conditions, electronic tunnelling between the two leads occurs only through virtual states on the oscillating wire.

In Paper I, the motion of the nanowire is treated quantum mechanically such that its frequency ω dictates the spacing between the quantised mechanical energy levels $\hbar\omega$ (see Section 2.1 and the discussion therein). By treating the nanowire quantum mechanically one necessarily has to take into account quantum fluctuations in its bending modes. Because of this, the electronic tunnelling paths are not localised to the one-dimensional nanowire, but will have a finite delocalisation in the direction transverse to the axis of it. This implies that electrons may tunnel through any path defined by the area swept out by the oscillating nanowire as illustrated in Fig. 5.2.

In the present analysis the magnetic field serves to alter the quantum phase acquired by tunnelling electrons, the effect of which depends on the path taken. Under such conditions, quantum interference effects in the electronic tunnelling become important for the overall charge transport. In Ref. [78] it was shown that the magnetic field couples the tunnelling electrons to the deflection operator $\hat{x} = x_0(\hat{b} + \hat{b}^\dagger)$, which implies that the coupling strength $\Phi \propto LHx_0$ is proportional to the area swept out by the oscillating nanowire. The coupling to the deflection operator further implies that the tunnelling electrons may change the quantum state of the oscillator, the outcome of which is analysed in Paper I. In other words, the energy of the tunnelling electrons may change due to interactions with the mechanical subsystem, such that not only the elastic (no change in energy) but also the inelastic absorption and

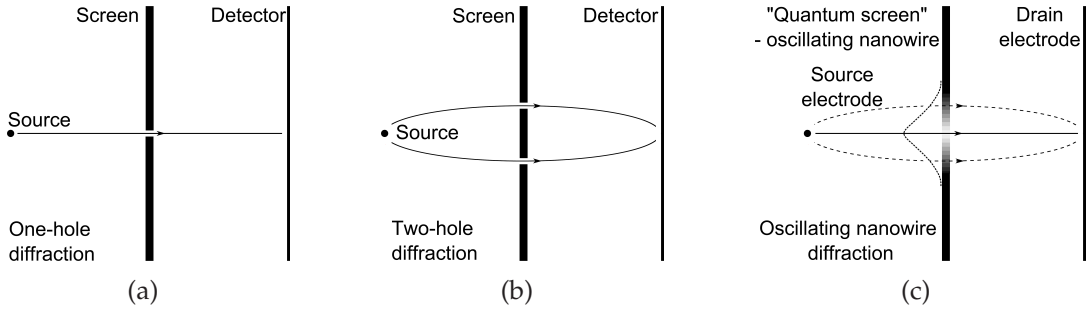

Figure 5.2: Illustration of electronic tunnelling paths due to quantum fluctuations of the nanowire. In (a) and (b) the quasiclassical analogue is presented where electrons pass through one or two holes in a screen before hitting the detector. In (b), the two holes result in quantum interference between the amplitudes of the two electron paths (solid arrows). In (c) the electrons pass through a "quantum hole", the position of which is determined by the fluctuations of the nanowire. The size of the hole effectively determines the magnitude of Φ. The tunnelling probability is high (solid) and low (dashed) depending on the path taken, which in turn depends on the probability of finding the nanowire at a given position (dashed profile).

emission channels (associated with $\hat{b}$ and $\hat{b}^\dagger$ respectively) are open.

In Paper I we analyse the effects of the electromechanical coupling on the charge transport through the junction. In doing so, we take into account not only the change in the tunnelling electrons due to the electromechanical coupling, but also consider the back-action on the system from the vibronic subsystem. These effects are relevant if the thermal damping of the nanowire is slow on the time scale of the electronic tunnelling rate, i.e. the vibronic subspace is driven into a non-equilibrium configuration due to the interactions with the electronic subsystem. Taking into account these effects we show that although inelastic electronic tunnelling may change the distribution of the vibrational modes, the high-voltage limit of the current follows that predicted below. These effects are discussed in some detail in Paper I and Appendix A and will not be discussed further here.

5.1.2 Pauli principle restrictions

As discussed above, each tunnelling electron will acquire a phase depending on the path taken. Due to the quantum fluctuations of the displacement of the nanowire, this results in a reduction of the elastic tunnelling current due to destructive quantum interference between the many electron tunnelling paths, see Fig. 5.2. In Paper I we show that the magnitude of this reduction implies that the current through the elastic channel I_0^{el} scales with the coupling constant Φ as $I_0^{el} \propto G_0 V \exp(-\Phi^2)$. Here, G_0 is the conductance at zero magnetic field (the subscript 0 indicates that we do not consider back-action effects from

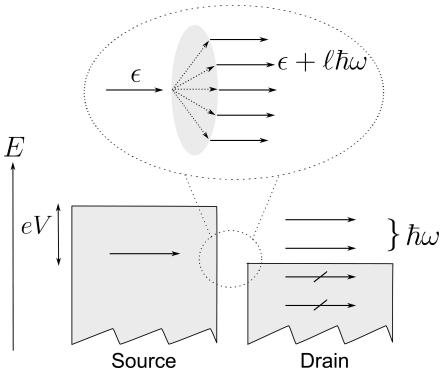

Figure 5.3: Allowed electronic tunnelling channels through the oscillating nanowire. Electrons with energy ϵ may tunnel from the source to the drain electrode through any of the open tunnelling channels $\epsilon + \ell\hbar\omega; \ell = 0, \pm 1, \pm 2, ...$ (top image). At low voltage-bias V, some of the inelastic channels are blocked at low temperature due to Pauli-principle restrictions which are set by the electronic population in the drain electrode (lower image). This, together with the suppression of the elastic $\ell = 0$ tunnelling channel, results in a reduction of the current through the system compared to the scenario of no electromechanical coupling.

the nanowire on the tunnelling current). Thus, the current over the wire from the elastic tunnelling channel is reduced from the current at zero magnetic field (no inelastic channels open) due to quantum interference effects between the tunnelling paths.

Not only the elastic, but also the inelastic tunnelling channels are however available in the present system. From our analysis we find that the inelastic channels will (if the electron distributions in the leads are neglected) exactly compensate the suppression of the elastic tunnelling current. Thus, the total current through the junction is given by the ohmic expression $I_0 = G_0 V$ if the quantum nature of the electron distributions in the leads are neglected.

In Paper I the effect of the quantum nature of the distribution of electrons in the leads on the overall charge transport is considered. This effect arises from the Pauli principle which states that no two electrons may occupy the same quantum state. These considerations are particularly important at low temperature when the electrons in the leads fill up all low-lying energy states in accordance with the so-called Fermi distribution.[2] Under such conditions, an electron which tunnels from one electrode may be blocked from entering the other electrode if it loses an amount of energy to the nanowire in the tunnelling process corresponding to the energy separation between two electrode as shown schematically in Fig. 5.3.

[2]The Fermi distribution gives the population of the electronic quantum states of a system as a function of temperature, equivalent to equation (2.3) for the vibrations of the quantum oscillator.

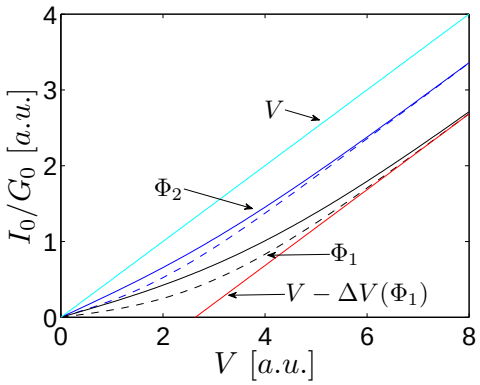

Figure 5.4: Current I_0/G_0 in arbitrary units for two coupling strengths Φ_1 (black) and Φ_2 (blue), $\Phi_1 > \Phi_2$, and two temperatures T_1 (solid) and T_2 (dashed), $T_1 > T_2$. The current deficit is given by the offset from the current at zero magnetic field V (cyan). Also shown is the constant voltage offset $V - \Delta V(\Phi_1)$ (red).

5.1.3 Current deficit

As discussed above, the quantum nature of the electronic distribution in the leads will introduce restrictions on the allowed inelastic electronic tunnelling channels. In particular we find that in the limit of large bias voltage $V \gg V_0$ the inelastic current (which compensates the suppression of the elastic channel) is reduced due to the Pauli principle restrictions on the low energy electrons. Here, $eV_0 \propto \max(k_B T, \hbar\omega\bar{\ell})$ is the voltage equivalent of the characteristic energy scale of the thermal energy $k_B T$ (which dictates the electronic distributions in the leads) and the energy of the average number of inelastic tunnelling channels $\hbar\omega\bar{\ell}$ which need to be considered where $\bar{\ell} \propto \Phi$.

These effects are illustrated in Fig. 5.3 where some of the inelastic channels are blocked for electrons with low energy. As the bias voltage is increased, proportionally more electrons can tunnel through any of the allowed inelastic channels thus compensating for the reduction of the elastic tunnelling channel. The number of forbidden low energy tunnelling channels is however fixed by the electromechanical coupling and the total current through the junction is reduced from the current at zero magnetic field by the corresponding number of blocked electronic tunnelling channels,

$$I_0(\Phi, V) = G_0\left(V - \frac{\hbar\omega}{e}\Phi^2\right) = I_0(0, V - \Delta V(\Phi))\,, \qquad V \gg V_0\,. \tag{5.1}$$

In the above the voltage offset $\Delta V(\Phi) = \hbar\omega\Phi^2/e$ gives the equivalent bias voltage necessary to recover the conductance through the system at zero magnetic field.

The analysis of Paper I predicts that the current I_0 is reduced from the current at zero magnetic field by an amount which depends on the number of

forbidden inelastic tunnelling channels according to equation (5.1). Alternatively, this corresponds to a voltage offset such that at potential bias $\Delta V(\Phi)$ is necessary in order to recover the ohmic transport regime. These effects are shown in Fig. 5.4 for two coupling strengths Φ_i and two temperatures. Note that in the high bias limit the current I_0 (black lines) follows that predicted by equation (5.1) (red line).

5.2 Paper II - Pumping the mechanical vibrations

In Paper II we consider the possibility to induce pumping of the vibrations of the suspended nanowire by connecting it to two voltage-biased superconducting leads in a low transparency junction. The presented analysis is primarily classical in that we analyse the equation of motion of the driven damped oscillator and discuss the resulting stability of the coupled electromechanical system. In particular we find that the motion of the nanowire in the magnetic field alters the time-evolution of the phase-difference, and show that this leads to the possibility to pump the vibrations of the nanowire under conditions of resonant bias voltage.[3]

5.2.1 Equation of motion

The dynamics of the nanowire (which is here treated as a damped classical harmonic oscillator) is described through its equation of motion. By considering a low transparency junction $D \ll 1$ the bound Andreev states which describe the electronic degrees of freedom in the system are widely separated and the current through the wire is to a good approximation given by the Josephson relation $j = j_c \sin\varphi$ where φ is the phase-difference and j_c is the critical current (see Chapter 3 and the discussion therein). This relation implies the current j through the wire will oscillate in time as the phase-difference changes due to the applied bias voltage V (see equation (3.1b)). The transverse magnetic field now serves two purposes. First, it will induce a force on the wire due to the current through it, the Lorentz force, which is proportional to the product LjH. Secondly, the motion of the wire in the magnetic field will induce an electromotive force which tries to oppose the motion causing it.[4] In Paper II we show that the expression for the electromotive force can be formally derived from the Bogoliubov-de Gennes equation which describes the electronic degrees of freedom of the superconducting junction (see Ref. [70] for details of this derivation). The outcome of this analysis is that the phase difference over the junction depends on the motion of the nanowire in the

[3]The inductive coupling between flexural wire vibrations and the supercurrent flow in a SQUID loop has been considered in Refs. [27, 79–81].

[4]This is Lenz's law which states that the induced current (or in this case phase) is always in a direction which is opposite to the change causing it.

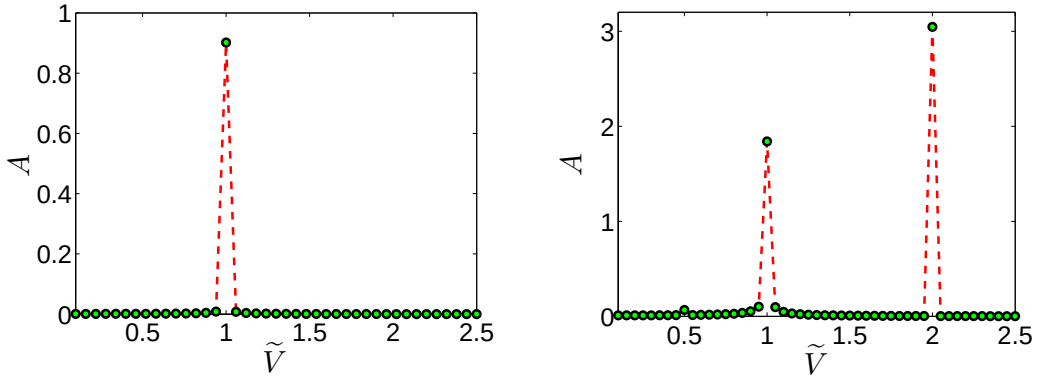

(a) $\epsilon \sim \widetilde{\gamma}$ (b) $\epsilon > \widetilde{\gamma}$

Figure 5.5: Numerical simulation of equation (5.2) for the time-averaged vibrational amplitude $A = \sqrt{\langle Y(t)^2 \rangle}$ as a function of the bias voltage $\widetilde{V}$ for two different driving strengths ϵ.

magnetic field $\dot{\varphi} \propto -LH\dot{a}$ where a is the vibrational amplitude of the wire. Alternatively this can be seen as the back-action on the electronic system from the motion of the nanowire in the magnetic field. Thus, the magnetic field determines both the force on the wire due to the flow of charge through it and the evolution of the phase difference due the motion of the wire. Formally this is described by the dimensionless equations of motion for the deflection coordinate Y and phase φ (for full definition of all parameters see Paper II),

$$\ddot{Y} + \widetilde{\gamma}\dot{Y} + Y = \epsilon \sin(\varphi)\,, \qquad \dot{\varphi} = \widetilde{V} - \dot{Y}\,. \tag{5.2}$$

Here, $\widetilde{\gamma}$ is the damping of the nanowire, $\epsilon \propto H^2L^2j_c$ is the driving strength and $\widetilde{V} \propto V/\omega$ where ω is the mechanical resonance frequency of the fundamental mode of the suspended nanowire.

5.2.2 Stability

The dynamics of the vibrating nanowire is governed by equation (5.2). Performing detailed numerical and analytical analysis we find that the effect of the electromechanical coupling is that the vibrations of the nanowire can be pumped to finite amplitude under resonant conditions. Furthermore, we find that this pumping not only occurs at the resonance frequency $\widetilde{V} = 1$ but also that the parametric resonance $\widetilde{V} = 2$ can be excited at higher driving force as displayed in Fig. 5.5(b). In Paper II we show that this behaviour is well explained through the two stability equations,

$$\dot{I}_n = -\widetilde{\gamma} I_n - 2\epsilon n J_n(\sqrt{I_n}) \sin\chi_n\,, \qquad \dot{\chi}_n = -\delta - 2\epsilon n J_n'(\sqrt{I_n}) \cos\chi_n\,, \tag{5.3}$$

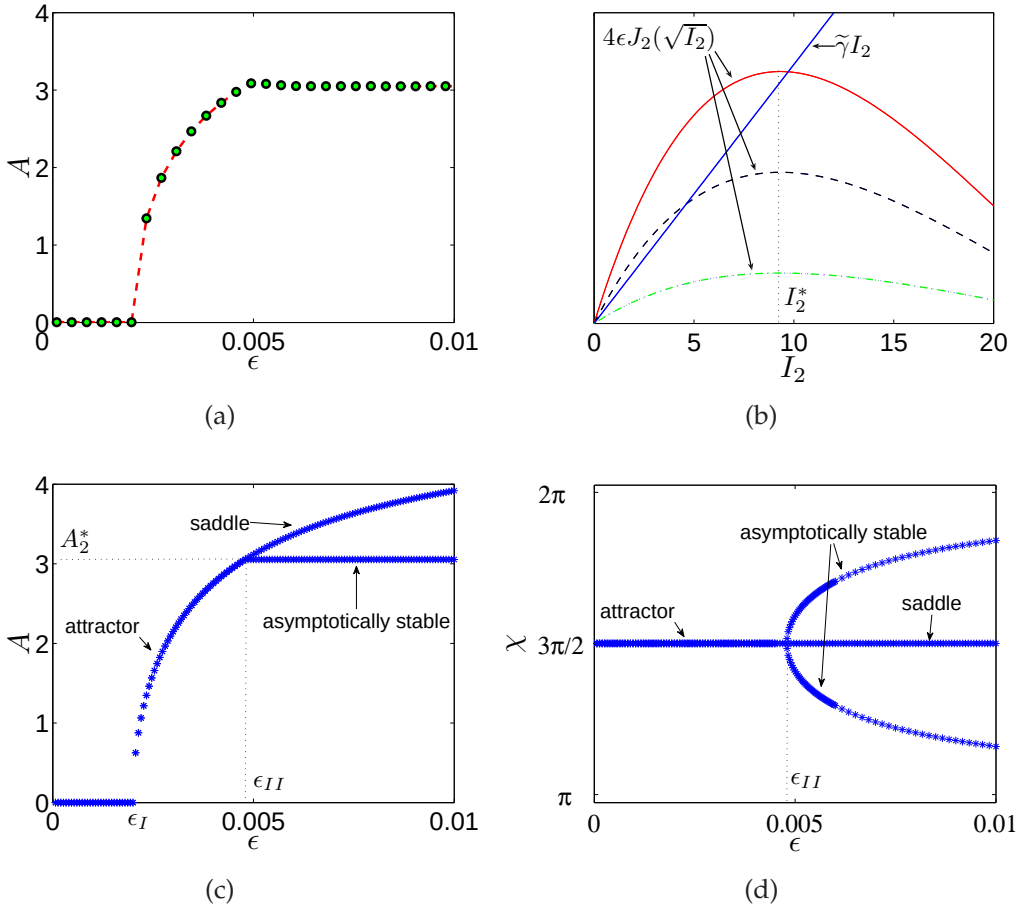

Figure 5.6: (a) Numerical simulation of the vibrational amplitude, equation (5.2), at the second resonance as a function of the driving strength. (b) Plot of the solution $\dot{I}_2 = 0$ in (5.3) for $\chi_2 = 3\pi/2$ for three different driving strengths, $\epsilon < \epsilon_I$ (dashed green), $\epsilon_I < \epsilon < \epsilon_{II}$ (dashed black) and $\epsilon > \epsilon_{II}$ (solid red). (c)-(d) Corresponding stability diagram for the amplitude and phase as a function of the driving strength.

where the amplitude I_n and phase χ_n are slow functions of time at resonance (see Appendix B for a derivation of the stability equations). In (5.3), J_n are Bessel functions of order $n = 1, 2, ...$ with $J_n^{'}$ being the derivative with respect to I_n and $\delta = \widetilde{V} - n$ measures the voltage offset from resonance.

The system considered will perform stable motion (vibrations with constant amplitude) if neither the amplitude I_n nor phase χ_n change in time, i.e. both equations (5.3) are simultaneously 0. At resonance, $\delta = 0$, this is found either at fixed phase $\cos\chi_n = 0$ or fixed amplitude $J_n'(\sqrt{I_n}) = 0$. For the parametric resonance $\widetilde{V} = 2$ such motion is only found once the driving force is $\epsilon \geq \epsilon_I = 2\widetilde{\gamma}$, whereas the first resonance peak is always present at finite driving. Also, the vibrational amplitude is initially an increasing function of the

driving force (for both peaks), which eventually saturates to finite vibrations once the driving force is $\epsilon \geq \epsilon_{II} = \widetilde{\gamma} I_n^* / (2nJ_n(\sqrt{I_n^*}))$ where I_n^* corresponds to the fixed amplitude solution $J_n'(\sqrt{I_n^*}) = 0$ as shown in Fig. 5.6(a).[5]

These phenomena are explained through the solution of equations (5.3). At $\delta = 0$ there always exists a solution $I_n = 0$ (no periodic vibrations of the wire). The stability of this solution is found by considering the expansion of the Bessel functions for small arguments I, $J_n(\sqrt{I}) \sim I^{n/2}$. With this one finds that the solution $I_n = 0$ is always unstable for $n = 1$ and becomes unstable for $n = 2$ at $\epsilon > \epsilon_I = 2\widetilde{\gamma}$. Thus, the peak at $\widetilde{V} = 1$ is always present for non-zero driving, whereas the peak at $\widetilde{V} = 2$ is only found once $\epsilon > \epsilon_I$ as shown in Figs. 5.6(a) and 5.6(c). At larger driving strengths $\epsilon > \epsilon_I$, the amplitude is an increasing function of ϵ (fixed phase solution) corresponding to the crossing of the two curves in Fig. 5.6(b). However, once the driving is large enough that this crossing moves past I_n^*, the fixed phase stability point becomes a saddle point and the system follows the trajectory of the fixed amplitude solution. This is shown in Figs. 5.6(c) and 5.6(d), from which we infer that the nanowire vibrates at the finite amplitude A_n^* for all $\epsilon > \epsilon_{II}$ if driven at resonance.

A final check of the validity of the stability analysis is to analyse the numerical solutions for the different resonance peaks (different n) at $\delta = 0$ over the type-I regimes. From (5.3) we expect the ratio $I_n/(n\epsilon J_n(\sqrt{I_n})$ to be constant for all peaks at a given $\widetilde{\gamma}$ in this regime. Comparing this with the numerical simulations we find excellent agreement.

Moving off resonance one finds the width of the peaks by solving for δ in equations (5.3),

$$\left(\frac{\widetilde{\gamma} I_n}{2\epsilon n J_n(\sqrt{I_n})}\right)^2 + \left(\frac{\delta}{2\epsilon n J_n'(\sqrt{I_n})}\right)^2 = 1\,. \tag{5.4}$$

For the parametric resonance $n = 2$ this implies that the total width of the peak is $2|\delta| = 2(\epsilon^2/4 - \widetilde{\gamma}^2)^{1/2}$. Furthermore, equation (5.4) has two stable solutions for the vibrational amplitude within the interval $(-\delta_c, \delta_c)$ at $\epsilon > \epsilon_{II}$. These solutions correspond to a separation of the fixed amplitude solutions in phase space with one solution being larger and the other smaller than the amplitude I_n^* at small $|\delta|$. This is shown in Fig. 5.7(b) for the second resonance peak. As $|\delta|$ is increased the solution which is larger than I_n^* merges with the saddle point (defined by the fixed phase solution) at $|\delta_c|$ and only one stable point (corresponding to the low amplitude solution) remains at larger $|\delta|$. The width of this window of bistability $2\delta_c$ scales as $(\epsilon - \epsilon_{II})^{3/2}$ as discussed in Appendix B.

[5]The notation I_n^* and $A_n^* = \sqrt{I_n^*}$ will be used interchangeably throughout this section. In Paper II these are referred to as A_0.

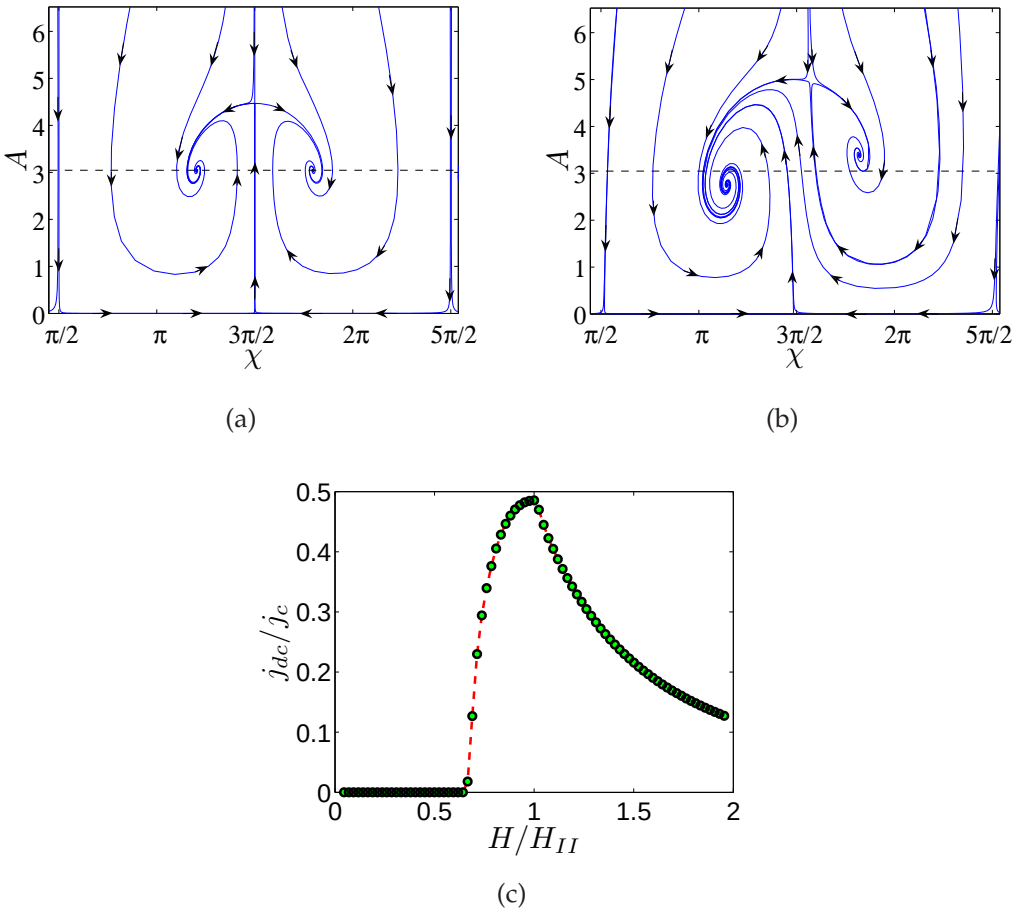

Figure 5.7: Phase space diagram for the second resonance peak at $\epsilon > \epsilon_{II}$. In (a) $\delta = 0$, two solutions can be found at the same amplitude. In (b) $0 < \delta < \delta_c$, the solutions are separate in phase-space. The dashed line corresponds to the fixed amplitude solution. (c) Current through the system at $\delta = 0$ at the parametric resonance as a function of the magnetic field. Here, H_{II} is the magnetic field corresponding to ϵ_{II}.

5.2.3 Current

The pumping of the mechanical vibrations draws energy from the battery connecting the junction. This implies a finite dc current j_{dc} over the junction. At resonance this current provides the energy necessary to compensate for the mechanical dissipation associated with $\widetilde{\gamma}$. Physically this implies that the current scales with the time-average velocity squared (see Appendix B for details). As the velocity $\dot{Y}$ and amplitude Y of the mechanical motion of the wire behave phenomenologically equivalent this implies that the system analysed in Paper II displays both positive and negative magnetoresistance.

To see this, consider at first the system when driven in the type-I regime, $\epsilon_I < \epsilon < \epsilon_{II}$. In this range, the amplitude is an increasing function of the magnetic field and the current correspondingly increases with H (negative magnetoresistance). However, once $\epsilon > \epsilon_{II}$ the vibrational amplitude saturates, and the current scales as H^{-2} under which conditions the system displays positive magnetoresistance. The transition between these two regimes is experimentally observable as a cusp as seen in Fig. 5.7(c).

5.3 Paper III - Voltage-biased cooling

In Paper III, the possibility to cool the vibrations of the oscillating nanowire in a voltage-biased superconducting junction (see Fig. 5.1) is considered. Unlike the experimental setup considered in Section 5.2, we here treat the oscillating nanowire as a quantum harmonic oscillator and furthermore consider the high-transparency limit of the nanowire junction. With these considerations we show that the transverse magnetic field can in the present situation result in magnetic-field induced transitions between the bound Andreev states describing the electronic degrees of freedom. These transitions are shown to be accompanied by the absorption of mechanical vibrons, which can effectively cool the nanowire below the ambient temperature.

5.3.1 Coupled electromechanical system

To describe the cooling process analysed in Paper III, consider at first the scenario when no coupling mediated by the magnetic field is present. Under such conditions, the nanowire will serve as a short metallic junction between the two superconducting leads. As discussed earlier, Section 3.3.1, superconductor-metal-superconductor junctions can sustain both normal and Andreev reflections at the metal-superconductor interface. This implies that the electronic degrees of freedom over the junction can be described through the formation of two bound Andreev states, the energy of which depend on the phase-difference ϕ according to $E_{\pm}(\phi) = \pm\sqrt{1 - D\sin^2(\phi/2)}$. The spatial

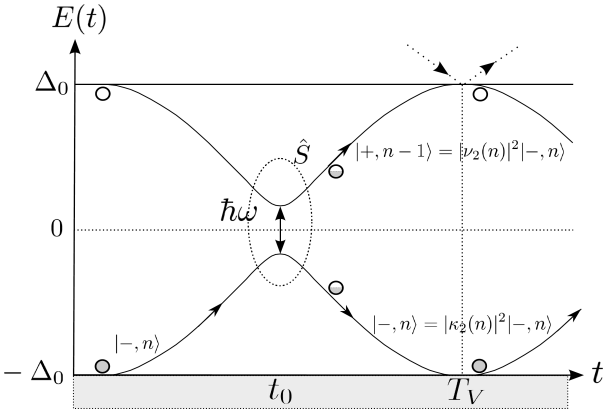

Figure 5.8: Schematic diagram of the evolution of the coupled electromechanical system. At the start of each period, two Andreev states are formed (empty and filled circle) from the quasiparticle spectrum in the superconducting leads. Due to the finite bias voltage, these evolve in time with a period T_V after which the Andreev levels are reset. The electromechanical coupling can promote transitions from the lower $|-\rangle$ to the upper $|+\rangle$ Andreev level through the absorption of one mechanical vibron $\hbar\omega$ ($|-,n\rangle \rightarrow |+,n-1\rangle$). In this process the nanowire is effectively cooled. Throughout the evolution of the system, the mechanical degrees of freedom are coupled to the thermal environment, whereas the electronic and mechanical degrees of freedom only interact during the short time $t \sim t_0$.

extent of these Andreev states will be of the order of the superconducting coherence length ξ which is here considered to be much larger than the length of the nanowire L.

Applying a bias voltage V across the junction will cause the phase difference to evolve in time according to equation (3.1b) and the bound Andreev states will follow the trajectories defined by $E_{\pm}(\phi(t))$. This is shown in Fig. 5.8 where the bound Andreev levels are indicated with the solid lines and the period of their evolution T_V depends on the bias voltage, $T_V = \pi\hbar/(eV)$. At the start of the period the population of the upper/lower Andreev level is dictated by the distribution of quasiparticle excitations in the superconducting leads. Here, we assume the external temperature to be low ($k_BT \ll 2\Delta_0$) which implies that the upper Andreev level will be virtually empty (empty circle) at the start the period as few quasiparticle excitations are found in the superconducting leads (cf. the discussion in Section 3.2). Similarly, the population of the lower level is close to unity at the start of the period (full circle). After one period, the bound Andreev states dissolve in the superconducting continuum and new states, which are orthogonal to the old states, are formed. In Paper III we assume that the electronic subsystem is reset at the start of each period. This is true if the excess energy released into the superconducting leads at the end of one period does not affect the formation of new Andreev levels at later periods. This assumption is justified for the experimental parameters used in

Paper III as discussed further in Appendix C.

As discussed in Chapter 3, the bound Andreev states carry current through the junction, the magnitude and sign of which is given by $2e/\hbar(\partial E/\partial\phi)$. Under conditions of adiabatic motion $eV \leq eV_c = 4R\Delta_0$, when the electronic system evolves slowly, the Andreev levels are superpositions of electronic states carrying current in opposite directions. In Paper III we show that the magnetic field couples the deflection of the nanowire to the current carried by the Andreev levels. Furthermore, we find that this results in an effective pairing between the two Andreev levels such that the electronic system can change from one level to the other through the absorption/emission of a mechanical vibron at resonant conditions. Alternatively this coupling can be derived by considering the change of the phase-difference due to the motion of the nanowire in the magnetic field, similar to the analysis of Paper II. This is discussed further in Appendix C.

In the present analysis the magnetic field serves to couple the two Andreev levels through the mechanical deflection operator $\propto \hat{b} + \hat{b}^\dagger$. Here, transitions from the lower to the upper Andreev level is considered only to proceed through the absorption channel associated with the operator $\hat{b}$, the so-called rotating wave approximation (RWA).[6] This type of transitions are greatly enhanced if the energy separation between the Andreev levels correspond to the energy scale set by the harmonic oscillator, $\hbar\omega$. Restricting our analysis to the region of maximal electromechanical coupling ($t \sim t_0$ in Fig. 5.8) this corresponds to the condition $2\Delta_0\sqrt{R} = \hbar\omega$ where $R = 1 - D$ is the electronic reflection probability. By considering realistic experimental parameters the mechanical energy is much smaller than the superconducting gap ($\hbar\omega \ll \Delta_0$), hence the predicted cooling phenomenon is only expected for high transparency junctions.

5.3.2 Adiabatic evolution of the Andreev levels

Formally, the dynamics of the coupled electromechanical system is described through its associated density matrix. In Paper III we analyse this evolution in the limit of high mechanical quality factor Q. This conditions implies that the mechanical subsystem only interacts weakly with the thermal environment.

To describe the evolution of the system the reader is referred to Fig. 5.8. For times $0 < t < t_0$ the electronic and mechanical degrees of freedom are decoupled. During this interval the electronic system (only the lower level is assumed to be populated) follows the trajectory defined by $E_-(\phi(t))$, whereas the mechanical subsystem interacts with the environment which brings it into thermal equilibrium at the rate $\gamma = \omega/Q$. At time $t = t_0$ the electromechani-

[6] In Ref. [71] the influence of emission stimulated transitions, non-RWA, is also considered and is shown to have little effect on the predicted level of cooling.

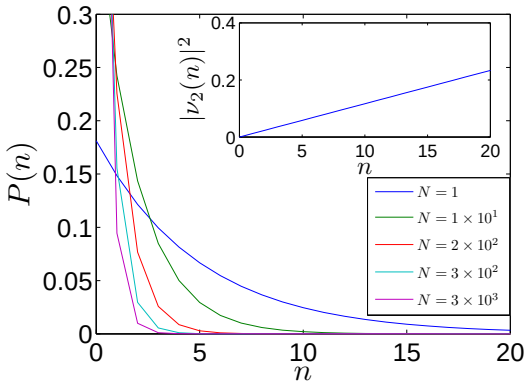

Figure 5.9: The distribution of the population of the vibrational modes $P(n)$ of the nanowire. In the above, N labels the number of periods and the inset shows the transition probability as a function of the number of the quantum state of the oscillator n. Here, the nanowire oscillator is cooled to its motional ground state $\langle n \rangle \lesssim 0.1$ after approximately 3000 periods (see Fig. 2.2(b) for reference).

cal interaction becomes significant, and the electronic subsystem may change (gain energy) through the absorption of a mechanical vibron. The probability of such transitions is $|\nu_2(n)|^2 \simeq \pi n \Gamma^2 \propto nH^2$ where Γ is the electromechanical coupling strength (see Paper III for full definitions). Note that the probability of transition depends on the quantum state of the oscillator n which follows from the coupling to the operator $\hat{b}$ (see also Appendix C). At times $t_0 < t < T_V$, the influence of the magnetic field is again negligible and the mechanical and electronic degrees of freedom are decoupled. Finally, the Andreev states are dissolved at the end of the period at $t = T_V$ and the electronic subsystem is reset. The mechanical subsystem is however not affected by the release of energy to the quasiparticle spectrum in the leads, and may be further cooled during the next cycle.

5.3.3 Ground-state cooling

Through the mechanism described in the previous section and in Fig. 5.8 the vibrations of the suspended nanowire may be cooled. The efficiency of this process depends on the competition between the probability of transitions between the Andreev levels and the thermal damping. Here, the magnetic field induced transitions are dictated by the coupling strength $\propto H$, such that strong coupling promotes transitions through the absorption channel and thus lowers the distribution of the vibrational modes $P(n)$. Similarly, weak coupling to the thermal bath, high Q, lowers the mechanical damping rate which act to bring the distribution of the vibrational modes back to thermal equilibrium. Finally, a slow evolution of the Andreev levels, low bias voltage V, implies a bigger resonance window and thus increased transition probability.

By evaluating the evolution of the coupled electromechanical system we calculate the average occupancy of vibrational modes $\langle n \rangle$ in the stationary regime, i.e. when the population of the vibrational modes does not change over one period. From this analysis we find that $\langle n \rangle$ is,

$$\langle n \rangle \propto \frac{n_B}{QH^2} \frac{\Delta_0}{\hbar\omega} \left(\frac{V}{V_c} \right)^{1/3} , \tag{5.5}$$

to lowest order in the small parameter $1/Q$. The corresponding evolution of the distribution of the vibrational modes is shown in Fig. 5.9, where the nanowire is cooled to its motional ground state $\langle n \rangle \sim 0.1$ (see Paper III for physical parameters). In (5.5), $n_B = (e^{\hbar\omega/k_B T} - 1)^{-1}$ is the corresponding average population of the vibrational modes in thermal equilibrium. The stationary distribution in Fig. 5.5 thus corresponds to,

$$\frac{\langle n \rangle}{n_B} \ll 1 , \qquad T_{\text{eff}} < T , \tag{5.6}$$

where T_{eff} is the "effective" temperature of the nanowire oscillator in the stationary regime.

In Ref. [71] the analysis of Paper III is extended to consider also how the transfer of energy from the mechanical to the electronic subsystem can be detected experimentally. In this paper, we show that the energy released into the superconducting leads should be experimentally observable through the associated dc current over the junction I_{dc}, which is proportional to the total transition probability $|\nu_2|^2$. Intrinsically this implies that the dc current scales with the average population $\langle n \rangle$,

$$I_{dc} = \langle n \rangle \Gamma^2 \frac{4e\Delta_0}{\hbar} \left(1 - \sqrt{R} \right) \propto \begin{cases} Q^{-1} & Q \gg 1 \\ 1 & Q \sim 1 . \end{cases} \tag{5.7}$$

In Fig. 5.10 the dependence of the current as a function of the mechanical quality factor is shown. Note, that in the limit of high quality factor, ground state cooling is predicted and the current scales inversely with Q. In the opposite limit, the mechanical subsystem equilibrates rapidly to the thermal background, hence the current is independent of Q.

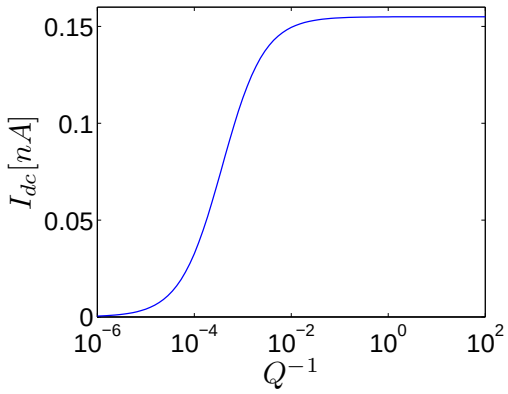

Figure 5.10: Lin-log plot of the current as a function of the inverse mechanical quality factor in the stationary regime, equation (5.7). At low Q, the current scales with the external temperature (independent of Q), whereas the high-Q limit scales with the population of the mechanical subsystem (inversely proportional to Q).

5.4 Paper IV - Cooling the vibrations in a current-biased junction

In Paper IV we study the current-biased equivalent of the system discussed in the previous section and in Paper III. Similarly to the analysis above, we consider the possibility to cool the mechanical vibrations of the nanowire through the absorption of mechanical vibrons by the electronic subsystem. In order to do so, we describe the electronic degrees of freedom through the so-called RCSJ-model and analyse the possibility to cool the vibrations of the nanowire through a phenomenon known as macroscopic quantum tunnelling.

5.4.1 The tilted washboard potential

In the RCSJ-model, the current-biased Josephson junction is modelled as a circuit element connected in parallel to a capacitance C and a resistance R as shown in Fig. 5.11(a). In this kind of junction the time-evolution of the phase-difference ϕ is described through an equation which is equivalent to that of a particle moving in a tilted cosine potential. This potential is usually referred to as the tilted washboard potential (see e.g. Ref. [33]) an example of which is shown in Fig. 5.11(b) where the tilting angle is proportional to the bias current I and the height and width of the valleys is determined from the physical parameters of the Josephson junction.

By changing the bias current the tilt of the washboard potential can be altered. In particular this implies that the phase ϕ can be highly localised to one of the minima of the potential if $\hbar I/(2e) < E_J$ where E_J the Josephson energy. If further $4E_c \ll E_J$ where $E_c = e^2/(2C)$ is the charging energy, the

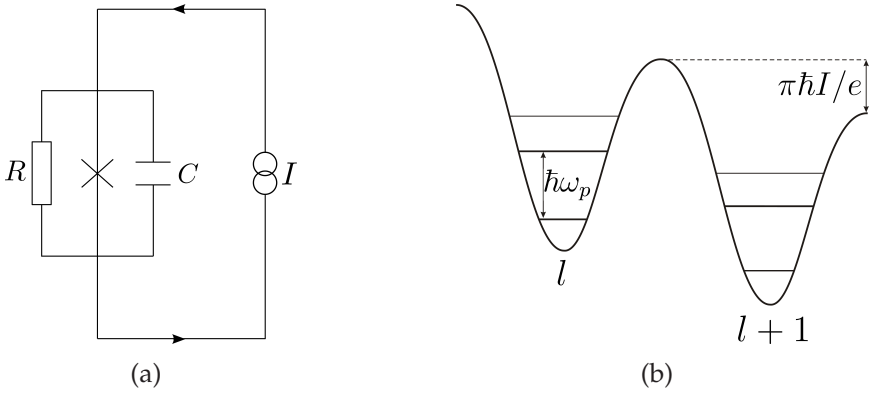

Figure 5.11: (a) The current biased Josephson junction. In the RCSJ-model, the Josephson junction (X) is modelled as being connected in parallel to a capacitance C and a phenomenological resistance R. In Paper IV, we consider the suspended nanowire to be part of the Josephson junction. (b) The tilted washboard potential for the electronic degrees of freedom. The equation of motion for the superconducting phase-difference ϕ corresponds to a particle in the above potential. If the bias current is small ($I < 2eE_J/\hbar$) the phase is localised inside the minima l of the potential. If further $4E_c/E_J \ll 1$, the phase effectively moves in a harmonic potential with quantised energy levels similar to those of the quantum harmonic oscillator. Here, ω_p is the plasma frequency.

equation of the phase is equivalent to that of a particle trapped in a virtually parabolic potential. Under such conditions, one expects quantised energy levels for the phase inside the valleys of the potential as indicated in Fig. 5.11(b) (see Ref. [82] for a more detailed discussion). Experimentally, this prediction has been confirmed in association with tunnelling of the phase from bound energy states within the potential minima of the washboard potential, a phenomenon known as macroscopic quantum tunnelling, see e.g. Refs. [83–85]. This kind of under-barrier tunnelling is the underlying cooling mechanism considered in this analysis.

In Paper IV we analyse how the coupling between the electronic degrees of freedom and the oscillating nanowire affects the dynamics of the system. The magnetic field is here considered to provide the electromechanical coupling in a similar way as in Papers II-III. Thus, we treat the motion of the short (compared to the superconducting coherence length) nanowire in the magnetic field as resulting in a modulation of the evolution of the phase-difference, $\hat{\phi} \to \hat{\phi} - \Phi(\hat{b} + \hat{b}^\dagger)$. Here, $\Phi \propto LH$ is the coupling constant, which we consider only to linear order in the analysis of Paper IV. In Appendix D the system Hamiltonian (equation (1) in Paper IV) is derived starting from the analysis of Paper II.

5.4.2 Macroscopic quantum tunnelling

As discussed above, the quantum state of the electronic system (the phase) may tunnel between consecutive valleys of the washboard potential. In Paper IV we consider this process to be the mechanism of cooling of the mechanical vibrations.

In order to analyse these tunnelling processes we perform a WKB calculation (see Ref. [82] for reference) for the overlap integrals for the elastic and inelastic tunnelling channels. From this analysis we find that the inelastic tunnelling channels $\propto \Phi(\hat{b} + \hat{b}^\dagger)$ are proportional to the elastic tunnelling amplitude $\mathcal{T}$ under conditions of strong quantisation, $4E_c/E_J \ll 1$. With this, we find that we may express the inelastic tunnelling amplitudes as $\Phi\mathcal{T}$, where the inelastic absorption [emission] channel is associated with the absorption [emission] of one quantum of energy $\hbar\omega$ from the mechanical to the electronic subsystem. This is shown in Fig. 5.12 where the absorption channel is assumed to be in resonance, i.e. the two bound energy states are separated by one quantum of mechanical energy $\hbar\omega$.

In Paper IV we analyse how the energy separation between the two levels involved in the tunnelling affects the overall level of cooling in the system. From this analysis we find that maximal cooling of the mechanical subsystem is achieved under conditions when the absorption channel is resonant as shown in Fig. 5.12. This condition corresponds to tuning the external bias current to $I = I^* - e\omega/\pi$ where $\omega_p = \sqrt{8E_J E_c}$ is the plasma frequency and $I^* = e\omega_p/\pi$ is the current which ensures that the lowest level in a given valley is resonant with the second level in the next valley. Here it should be noted that the minima of the potential are only to first approximation parabolic. This implies that the energy levels within each valley are not evenly distributed. Because of this we neglect all but the two lowest energy levels in the present analysis as the overlap between the higher energy levels will be small if the energy separation between the two lowest levels is of the order of $\hbar\omega$ (for experimental parameters $\omega \ll \omega_p$). Note also, that the anharmonicity of the washboard potential slightly changes the conditions for the bias current to be resonant as discussed in Appendix D

Interactions with the electronic quasiparticle environment in the leads introduce damping to the electronic subsystem. In Paper IV, these effects are included through the phenomenological resistance R, see Fig. 5.11(a), which we treat as a perturbation to the evolution of the electronic system. In Fig. 5.12 the damping is modelled as the decay of the electronic system from the higher to the lower level within a given valley. Here, $\Gamma = 1/(RC)$ is the electronic decay rate, see e.g. Ref. [86]. For the parameters considered in Paper IV, the electronic damping rate is greater than the tunnelling rate, $\Gamma > \mathcal{T}/\hbar$. This implies that the system, once it has tunnelled to the higher level in a given valley, is more likely to decay to the lower level than it is to tunnel back to the previ-

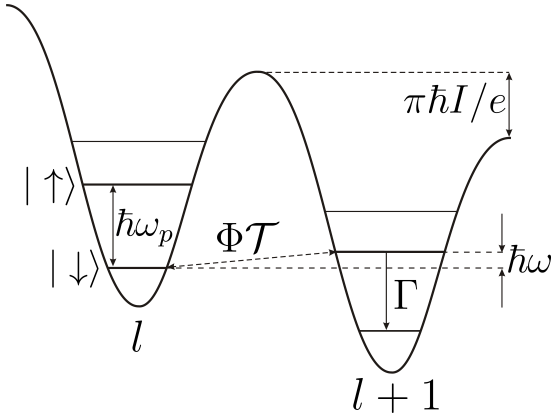

Figure 5.12: Macroscopic quantum tunnelling. The electronic subsystem may tunnel from one bound state in the valley l to another bound state in $l+1$. Such tunnelling is greatly promoted if the levels are resonant. Here, the system originally in the quantum state $|l,\downarrow\rangle$ tunnels to the state $|l+1,\uparrow\rangle$ through the absorption of a mechanical vibron (absorption channel) with $\Phi\mathcal{T}$ the inelastic tunnelling amplitude. Interactions with the quasiparticle environment in the leads causes the electronic system to decay from the upper to the lower level in a given valley at the rate Γ.

ous valley. Furthermore, the interactions with the quasiparticle environment lead to broadening of the quantised energy, which implies that not only the resonant channel is open. In Paper IV this is accounted for by considering all (absorption, elastic and emission) tunnelling channels in the analysis of the evolution of the system.

5.4.3 Ground state cooling

The mechanism of cooling discussed in Paper IV relies on the possibility to promote tunnelling through the absorption channel over the emission channel. This can be achieved by tuning the current bias as discussed above. In our analysis we show that this may result in ground-state cooling of the oscillating nanowire if the equivalent of the resolved sideband limit $\omega > \Gamma$ can be realised (cf. Section 2.3.1). To show this, we perform a perturbative calculation for the stationary solution of the density matrix. From this analysis we find that the level of cooling of the mechanical subsystem scales with the ratio between the tunnelling rates of the emission (Γ_+) and the absorption (Γ_-) channel. Here, the tunnelling rates are given by,

$$\Gamma_i = \frac{4\Gamma\mathcal{T}_i^2}{4(\Delta\mathcal{F}_i)^2 + \hbar^2\Gamma^2}\,, \tag{5.8}$$

$$\mathcal{T}_i = \begin{cases} \Phi\mathcal{T} & i=\pm \\ \mathcal{T} & i=0\,, \end{cases} \qquad \Delta\mathcal{F}_i = \begin{cases} \mathcal{F}_{l+1,\uparrow} - \mathcal{F}_{l,\downarrow} \pm \hbar\omega & i=\pm \\ \mathcal{F}_{l+1,\uparrow} - \mathcal{F}_{l,\downarrow} & i=0\,, \end{cases}$$

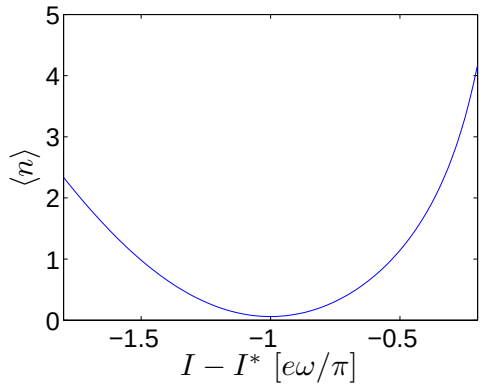

Figure 5.13: Stationary average vibron population as a function of the current bias. At $I - I^* = -e\omega/\pi$, the absorption channel is resonant and maximal cooling of the mechanical subsystem is achieved.

where the subscript 0 corresponds to the elastic channel and $\mathcal{F}_{l,\downarrow\uparrow}$ are the quantised energy levels for the electronic degrees of freedom (see Paper IV and Appendix D for full definitions). Note that the expressions given in (5.8) corresponds to the tunnelling rate between the lower levels in two adjacent valleys through the intermediate upper state.

In Paper IV we include also effects of the external temperature in the analysis of the suggested cooling mechanism. Including these effects we find, as expected, that the thermal damping rate reduces the level of cooling of the mechanical subsystem. With these considerations we calculate the stationary average vibron population of the mechanical subsystem,

$$\langle n \rangle = \frac{n_B\gamma + \Gamma_+}{\Gamma_- + \gamma - \Gamma_+} \ll n_B\,, \qquad \Gamma_- \gg \Gamma_+\,. \tag{5.9}$$

In Fig. 5.13, the stationary average occupancy of the mechanical subsystem is shown as a function of the current bias. The level of cooling we suggest to probe through the associated potential drop V over the junction. Here, V is calculated from the evolution of the phase down the tilted washboard potential through consecutive macroscopic tunnelling events ($V \propto \dot{\phi}$),

$$V = \frac{\pi\hbar}{e}(\Gamma_0 + \Gamma_-\langle n \rangle + \Gamma_+(\langle n \rangle + 1))\,. \tag{5.10}$$

Note that the potential drop scales with the elastic tunnelling rate (independent of the mechanical subsystem) and the average vibron occupancy.

CHAPTER 6

Conclusion

The material presented in this thesis summarises my work as a PhD student at the University of Gothenburg. In writing the thesis I have made a conscientious effort to present my work at a level which is hopefully, at least in part, accessible to an audience with only a limited background in physics. This is aimed to serve as an introduction to the appended papers on which the thesis is centred. In these, more details on the motivation, derivation and discussion of the results is presented.

My work as a PhD student has focused on quantum mechanical effects on charge transport in suspended nanowire structures. In particular, we have analysed the effects of magnetic field-induced interactions between the transport of charge carriers and the mechanical vibrations of the nanowire under various experimental setups. Throughout, the focus of my work has centred on phenomenological effects of the electromechanical interactions in these systems in order to highlight possible new phenomena related to the charge transport and the mechanical motion of the nanowires.

In particular, the presented material introduces three novel mesoscopic effects on charge transport in suspended nanowire systems. In the first work, we study how the vibrations of a suspended nanowire alter the electronic tunnelling paths over it, and show that this results in an interference phenomenon similar to the Aharanov-Bohm effect caused to the transverse magnetic field. The outcome of this analysis is a temperature- and bias voltage-independent current deficit (voltage offset) as compared to the current at zero magnetic field.

The second phenomenon discussed presents an analysis of the possibility to pump the vibrations of a suspended nanowire in a low-transparency superconducting weak link. This effect is shown to derive from the modulation of the phase-difference between the superconductors due to the motion of the nanowire in the magnetic field. In our analysis we show that this may result in pumping of the vibrations of the nanowire under resonant bias voltage conditions. Furthermore, our analysis shows that the vibrational amplitude of the nanowire may be driven into a region of bistability, which may be probed experimentally through the associated current over the junction.

In the final section of the thesis two different mechanisms to cool the quan-

tised vibrations of a suspended nanowire is considered. These are shown to derive in the first place from magnetic field induced transitions between bound Andreev levels in a voltage-biased high-transparency junction. In the second case, the current-biased equivalent system is analysed where the effect of the electromagnetic coupling (mediated through the magnetic field) is shown to promote inelastic macroscopic tunnelling of the superconducting phase under resonant current-bias conditions. For both systems considered ground-state cooling of the mechanical subsystem is predicted.

It is my hope that the presented work may inspire other groups, theoretical and experimental, working within the field of nanoelectromechanics to pursue the thoughts and concepts presented in this thesis. As with much of science, making predictions about where your field will end up is tricky as new hurdles are constantly encountered as old ones are eliminated. I do believe that the field of ground-state cooling will continue to be very active, with the hope that we will sooner or later find a stable, reproducible method to achieve this with small, high-quality mechanical oscillators. If this can be achieved we will perhaps one day be able to manipulate things small enough that "[...] mechanical engineers will have to include $\hbar$ among their list of standard engineering constants." [11], however I believe that this day is still somewhere in the not too near future.

Acknowledgement

Now to the part of the thesis which people will probably read first. First and foremost I would like to thank my supervisor Leonid Gorelik without whom I would not be here today. I am very grateful for the time you have dedicated to me and my work, as well as your efforts in explaining physics to me. Also, I am proud to be your first official PhD student to graduate. I know that I speak not only for myself, but for many previous PhD students in the group, when I say that your help makes all the difference.

Secondly I would like to thank my examiner Mats Jonson and assistant supervisor Robert Shekhter for all their help. Writing a paper is a process which involves many steps. Without your insightful comments, both relating to the physics and the way the material is presented, I would not have been able to publish my results to the same level and extent. Also, I would like to give an extra thank you to Mats for always supporting and encouraging me to go to different summer schools and conferences. This has been most appreciated and I have learnt a lot from it.

I would like to give a big thank you to the CMT group for making my years as a PhD student so enjoyable. The banter around the coffee table will perhaps not always focus on topics related to physics — rather we seem to put a lot of our energy into discussing religion — but it never fails to amuse me. What makes coming to work in the morning fun is very much down to the people you work with. I consider myself lucky to have been part of a group where this is the case.

A big thank you to Fabio, with whom I have shared office over the last five years. You taking your time to discuss topics related to my research or courses is most appreciated. Not to mention your amusing anecdotes about Berlusconi and Italian bureaucracy, which always makes me smile. Also, I would like to thank my fellow PhD students in the group. Yury, Robert, Magnus, Aurora, Caroline, Juan, Eduardo, Anders and Daniel, you make coming to work fun. Many of you have also helped me with various things over the years for which I am most grateful. A big thank you also to the rest of the CMT group — Andreas, Jari, Peter, Marina, Danko, Raffaello, Mattias, Anatoly, Weihua, Tomasz and Hee-Chul — for your support and company during the years.

As a graduate student I have had the pleasure of meeting many fellow PhD

students from other groups and departments. Of these I would in particular like to mention Erika and Anton. Erika, the ice cream making was at times tiresome, but with your company it was the best teaching assignment during my years at GU. And Anton, thank you for dragging me along the "Svensk klassiker". I know I would not have put in the same number of hours training if I did not know you were doing twice as much. I would also like to give a big thank you to the department secretaries Rose-Marie Wikström and Bea Augustsson for taking such good care of us. My questions have over the years been many and at times annoying, but you have always been very welcoming and helpful towards me. Additionally, I would like to give a special thank you to Rose-Marie for all your efforts in making the department a better place for the PhD students, a benefit I fear future students will have to do without.

A big thank you also goes out to all my friends who have helped me keep my spirits up over the years. In particular I want to thank Philip for dragging me along to the gym when I needed it the most (not to mention all the nice food you have presented over the years). A big thanks also to Patrik, Linnea, Sanita and Thomas for making my years in Gothenburg so enjoyable. Last but not least, my friends from Edinburgh deserve a special acknowledgement. Rob, Owen, Pete, Steve, Amanda, Anja and Klas, thanks for making it four very enjoyable years. Who would have thought Thirlestane road would take me here?

Finally, I would like to give a big thank you to my family as well as to the Wadells for all their support. This thesis is very much dedicated to you. And Tove. Thank you for coming into my life. You make me very happy and I am fortunate to have met you.

APPENDIX A

Supplement to Paper I

Evolution of the density matrix

The formal solution for the evolution of the total density matrix in the interaction picture is ,

$$\frac{\partial\hat{\tilde{\sigma}}(t)}{\partial t} = -\frac{i}{\hbar}[\hat{\tilde{H}}_T(t), \hat{\tilde{\sigma}}(0)] - \frac{1}{\hbar^2}\int_0^t \mathrm{d}t'[\hat{\tilde{H}}_T(t), [\hat{\tilde{H}}_T(t'), \hat{\tilde{\sigma}}(t')]]\,, \tag{A.1}$$

see Ref. [87] for a more detailed discussion and Paper I for definitions. Tracing out the leads with $\hat{\tilde{\sigma}}(t) = \hat{\tilde{\rho}}(t)\hat{\sigma}_{\text{leads}}$ under the assumption that the distributions in the leads $\hat{\sigma}_{\text{leads}}$ is constant in time and $\text{Tr}_{\text{leads}}(\hat{\tilde{H}}_T(t)\hat{\sigma}_{\text{leads}}) = 0$, we have

$$\frac{\partial\hat{\tilde{\rho}}(t)}{\partial t} = -\frac{1}{\hbar^2}\text{Tr}_{\text{leads}}\left(\int_0^t \mathrm{d}t'[\hat{\tilde{H}}_T(t), [\hat{\tilde{H}}_T(t'), \hat{\tilde{\sigma}}(t')]]\right)\,. \tag{A.2}$$

From equation (A.2) it follows that the evolution of the reduced density matrix in the Schrödinger picture is given by equation (6) in Paper I. The stationary solution to this equation naturally gives the definitions of the operators $\hat{J}_{1,2}$.

Back-action current

As outlined in Paper I the current operator $\hat{I}$ can be derived from,

$$\hat{I} = e\frac{\partial\hat{N}_l}{\partial t} = \frac{ie}{\hbar}[\hat{H}, \hat{N}_l]\,, \tag{A.3}$$

where $\hat{N}_l$ is the number operator in the left (high-bias) lead. Evaluating this we find that the average mechanical deflection of the wire is proportional to the average Lorentz force on it. This in turn may be compared to the equivalent expression,

$$k\langle\hat{x}\rangle = |T_{\text{eff}}|^2\hbar\chi\text{Tr}\left[\left(\hat{J}_r - \hat{J}_l\right)\hat{\rho}\right]\,, \tag{A.4}$$

which relates the mechanical deflection to the operators $\hat{J}_i$. From this, the current is found from $I = \frac{1}{2}e|T_{\text{eff}}|^2\text{Tr}\left[\left(\hat{J}_r - \hat{J}_l\right)\hat{\rho}\right]$.

To calculate the diagonal contributions to the current as given by equation (10) in Paper I, one may evaluate the above by tracing out all diagonal parts. This analysis eliminates the time-dependence in the operators $\hat{J}_i$ and the energy of the Fermi functions is shifted with respect to the energy transfer between the electronic and mechanical subsystems. In particular one finds that electronic tunnelling with the exchange of energy to/from the mechanical subsystem is only possible if the corresponding energy state in the lead into which the electron tunnels is not already occupied. This is indicated by the combinations of Fermi functions, e.g. $f_l(\epsilon)(1-f_r(\epsilon-\ell\hbar\omega))$, in equation (10) in Paper I.

To evaluate the off-diagonal parts we expand the expression for I_1 (equation (11) in Paper I) in powers of $\hat{H}_0\tau$. With this we find,

$$\hat{J}_1 = -\frac{\nu^2}{\hbar}\int \mathrm{d}\epsilon_1\mathrm{d}\epsilon_2 \int_{-\infty}^{0} \mathrm{d}\tau f(\epsilon_1)(1-f(\epsilon_2))e^{i\tau(\epsilon_1-\epsilon_2+eV)}\times \sum_{q=0}^{\infty}\frac{(i\tau)^q}{q!}e^{i\chi\hat{x}}\hat{Y}(\hat{H}_0, e^{-i\chi\hat{x}}, q)\,, \tag{A.5}$$

where $\epsilon_{1,2} = \epsilon_{r,l} \pm \frac{1}{2}eV$ and $f_{r,l}(\epsilon) = f(\epsilon \pm \frac{1}{2}eV)$. With the above, one can evaluate the integrals over energy ϵ_i by closing the contours in the complex plane (see Ref. [88] for details),

$$\int \mathrm{d}\epsilon f(\epsilon)e^{-i\epsilon\tau} = \int \mathrm{d}\epsilon(1-f(\epsilon))e^{i\epsilon\tau} = \pi\left(\delta(\tau) + \mathrm{PV}\left(\frac{i}{\beta\sinh(\pi\tau/\beta)}\right)\right)\,. \tag{A.6}$$

Equation (A.5) may thus be evaluated at all order τ. In particular one finds that the first order corrections in τ scale with the average momentum $\langle p\rangle$, which is zero according to equation (8b) in Paper I. The higher order corrections are found by collecting contributions at the same order in τ from all four components $\hat{J}_i$. With this the current I_1 reads,

$$I_1 \propto \frac{\nu^2\pi^2}{\hbar\beta^2}\int_{-\infty}^{0}\mathrm{d}\tau\frac{1}{\sinh^2(\pi\tau/\beta)}\sum_{q=2}^{\infty}\sum_{k=0}^{q-2}\binom{q}{k}\frac{1}{q!}\left(\frac{i\tau\hbar\chi}{2m}\right)^q(\chi\hbar)^k 2^{q-k}\langle\hat{p}^{q-k}\rangle\times \begin{cases}\sin(eV\tau) & q=\text{odd}\\ \cos(eV\tau) & q=\text{even}\,.\end{cases} \tag{A.7}$$

Here, the moments of the momentum $\langle\hat{p}^q\rangle$ are polynomials in the bias voltage at all orders q. With this we find that the contributions from the back-action current to the total current will decay exponentially as the above scale as $(\exp(\beta eV)-1)^{-1}$ in the limit $\beta eV \gg 1$.

APPENDIX B

Supplement to Paper II

Stability equations

Starting from equation (5.2), the stability equations (5.3) can be found by introducing the anzats $Y(t) = \sqrt{I_n(t)}\sin\Theta((t))$ where $\Theta(t) = \widetilde{V}t/n + \chi_n(t)/n$. Close to resonance both the amplitude I_n and phase χ_n are slow functions of time. Substituting the expression for $Y(t)$ into (5.2) we find two equations which govern I_n and χ_n when $\widetilde{V} \simeq n$. Integrating these over the period Θ, we arrive at the stability equations of the system (5.3),

$$\dot{I}_n = -\widetilde{\gamma} I_n + 2n\frac{\partial \mathcal{H}_{\text{eff}}}{\partial \chi_n}\,, \qquad \dot{\chi}_n = n - \widetilde{V} - 2n\frac{\partial \mathcal{H}_{\text{eff}}}{\partial I_n}\,,$$
$$\mathcal{H}_{\text{eff}} = \frac{\epsilon}{2\pi}\int_{-\pi}^{\pi}\cos(n\Theta - \chi_n - \sqrt{I_n}\sin(\Theta))\mathrm{d}\Theta\,,$$
$$\mathcal{H}_{\text{eff}} = \epsilon J_n(\sqrt{I_n})\cos(\chi_n)\,. \tag{B.1}$$

Scaling of bifurcation with the magnetic field

To find the scaling of the bifurcation amplitude with the magnetic field we expand the solutions of (5.3) close to the transition from the constant phase to the constant amplitude solution, i.e. we consider $\epsilon = \epsilon_{II} + \Delta\epsilon$ with $\Delta\epsilon \ll \epsilon_{II}$.

At $\epsilon = \epsilon_{II}$ the stable solution is given by $J_n(\sqrt{I_n^*}) = 0$ and $\chi_n^* = (2n-1)\pi/2$. Expanding the solution about this point we find,

$$-\widetilde{\gamma}\Delta I_n + 2n\Delta\epsilon J_n(\sqrt{I_n^*}) = \frac{J_n(\sqrt{I_n^*})\delta^2}{4n\epsilon_{II}|J_n''(\sqrt{I_n^*})|^2(\Delta I_n)^2}\,, \tag{B.2}$$

where $\Delta I_n = I_n - I_n^*$. Note that in the above $\widetilde{\gamma}$ is uniquely defined by ϵ_{II} through $\widetilde{\gamma} = 2\epsilon_{II}nJ_n(\sqrt{I_n^*})/I_n^*$. From equation (B.2) we calculate the maximum separation in the vibrational amplitude which is found from the zeros of the cubic equation,

$$\left(\Delta I_n - \frac{2\alpha}{3}\right)^2(-\Delta I_n - \frac{\alpha}{3}) = 0\,, \qquad \alpha = \frac{2n\Delta\epsilon J_n(\sqrt{I_n^*})}{\widetilde{\gamma}}\,. \tag{B.3}$$

With this, the maximum separation in amplitude between the two solutions scale as $I_n^*\Delta\epsilon/\epsilon_{II}$. Furthermore, it can be shown that,

$$\frac{\delta^2 J_n(\sqrt{I_n^*})}{4n\epsilon_{II}|J_n''(\sqrt{I_n^*})|^2\widetilde{\gamma}} = \frac{1}{2}\left(\frac{2\alpha}{3}\right)^3 , \tag{B.4}$$

which implies that we can solve for δ,

$$\delta = (\Delta\epsilon)^{3/2}\left(\frac{2I_n^*}{3\epsilon_{II}}\right)^{3/2}\left(\frac{2n\epsilon_{II}|J_n''(\sqrt{I_n^*})|^2}{I_n^*}\right)^{1/3} , \tag{B.5}$$

to find to find that the width of the window of bistability scales with the magnetic field as H^3 close to the region of bifurcation.

Current

The dc current through the system is calculated by considering the energy dissipation due to the damping of the mechanical vibrations. This can be shown by multiplying (5.2) throughout by $\dot{Y}$ and averaging over time. At resonance, the total energy associated with the harmonic oscillator $E \propto \dot{Y}^2 + Y^2$ does not change in time. This implies that the total energy dissipated by the mechanical system $\widetilde{\gamma}\langle\dot{Y}^2\rangle$ is related to the current drawn from the battery according to,

$$\widetilde{\gamma}\langle\dot{Y}^2\rangle = \frac{\epsilon}{T}\int_{-T/2}^{T/2}\dot{Y}\sin(\widetilde{V}\tau - Y)\mathrm{d}\tau\,, \qquad \tau = \omega t\,. \tag{B.6}$$

Evaluating the right hand side of (B.6) we eliminate the dependence of $\dot{Y}$ and find,

$$\widetilde{\gamma}\langle\dot{Y}^2\rangle = \epsilon\widetilde{V}\frac{j_{dc}}{j_c}\,. \tag{B.7}$$

The corresponding expression for the dc current j_{dc} is,

$$j_{dc} = \frac{\widetilde{\gamma}\langle\dot{Y}^2\rangle m\hbar\omega^2}{8eL^2H^2\widetilde{V}} = \frac{\gamma\langle\dot{a}^2(t)\rangle}{V}\,. \tag{B.8}$$

APPENDIX C

Supplement to Paper III

Induced Andreev level transitions

An alternative derivation for the electromechanical coupling is presented below. Starting from the electronic Hamiltonian $\hat{H}(\phi)$ (see Paper III for definitions),

$$\hat{H}(\phi) = \Delta_0 \cos(\phi/2)\hat{\sigma}_z + \Delta_0\sqrt{R}\sin(\phi/2)\,, \tag{C.1}$$

we consider the effects of the motion of the nanowire in the magnetic field. Similarly to the analysis of Paper II, this analysis shows that the motion of the nanowire changes the phase difference ϕ over the leads according to $\phi \to \phi - \tilde{\Phi}\hat{y}$. Here, $\tilde{\Phi} = \Phi/y_0$. In the following only linear terms in the small parameter $\tilde{\Phi}\hat{y}$ are considered.

Next we performing a rotation to the basis of the Andreev states considered in the paper,

$$\begin{aligned}
&\hat{\mathbb{H}} = e^{i\lambda\hat{\sigma}_y/2}\left(\hat{H}(\phi-\tilde{\Phi}\hat{y}) + \frac{\hat{p}_y^2}{2m} + \frac{m\omega\hat{y}^2}{2}\right)e^{-i\lambda\hat{\sigma}_y/2}\,, \qquad \tan(\lambda) = \sqrt{R}\tan(\phi/2)\,,\\
&\hat{\mathbb{H}} = \Delta_0\sqrt{1-D\sin^2(\phi/2)}\hat{\sigma}_z + \Delta_0\frac{\sqrt{R}\tilde{\Phi}\hat{y}}{\sqrt{1-D\sin^2(\phi/2)}}\hat{\sigma}_x + \\
&\qquad\qquad \Delta_0\frac{\tilde{\Phi}\hat{y}(1-R)\sin(\phi)}{2\sqrt{1-D\sin^2(\phi/2)}}\hat{\sigma}_z + \frac{\hat{p}_y^2}{2m} + \frac{m\omega\hat{y}^2}{2}\,.
\end{aligned} \tag{C.2}$$

In the above, the off-diagonal coupling $\propto \hat{\sigma}_x$ is small except when $\phi = \pi$ in which instance maximal coupling $\Delta_0\tilde{\Phi}\hat{y}$ is achieved. Note, also that $\hat{\mathbb{H}}$ contains a term $\propto \hat{y}\hat{\sigma}_z$. This term is however ignored in the present analysis due to the large separation in energy scales $\hbar\omega \ll \Delta_0$, which forbids inter-level transitions outside of the resonance window $\phi \simeq \pi$, at which point the diagonal dependence on $\hat{y}$ is identically zero.

Transition probability

Starting from equation (4) in Paper III, the expression for $|\nu_2(n)|$ can be derived by considering the probability that the state initially in the lower branch at

time $\tau = -\delta\tau$ scatters into the upper state after passing through the resonance. Formally this is done by solving equation (4) in Paper III with

$$c_{+,n-1}(\tau) = \delta c_{+,n-1}(\tau)\,, \qquad c_{-,n}(\tau) = c^0_{-,n}(\tau) + \delta c_{-,n}(\tau)\,, \qquad \tau > -\delta\tau\,, \quad \text{(C.3)}$$

where $|c^0_{-,n}(-\delta\tau)|^2 = 1$ is the unperturbed solution, i.e. the electronic subsystem is found in the lower Andreev branch with unit probability. Substituting (C.3) into equation (4) of Paper III we find the solution for $|\delta c_{+,n-1}(\delta\tau)|^2$ which corresponds to the transition probability $|\nu_2(n)|^2$,

$$|\nu_2(n)|^2 = |\delta c_{+,n-1}(\delta\tau)|^2 = \left|\Gamma\sqrt{n}e^{-i\delta\tau^3/3}\int_{-\delta\tau}^{\delta\tau} e^{2i\Lambda^3/3}\mathrm{d}\Lambda\right|^2 . \quad \text{(C.4)}$$

Energy release to the leads

As was discussed in some detail in Ref. [89], the state which dissolve at the edge of the quasiparticle spectrum $E = \pm\Delta_0$ cannot evolve dynamically into the new Andreev state, which moves away from the edge after it has formed. This follows from the fact that the two state are orthogonal to each other, hence the Andreev states are "reset" at the start of each period with unitary efficiency. This condition only applies if the populations of the superconducting leads remain unchanged, i.e. the bound Andreev states are formed from the same quasiparticle spectrum at each period. In order for this to be true, any excess energy released from the Andreev states into the superconducting leads at the end of the period must be removed from the junction during the period of the evolution of the Andreev levels, T_V.

To show this, we consider the characteristic energy of the quasiparticles created in the superconducting continuum close to the edge of the Andreev period,

$$\delta E = E(t = 2\pi) - E(t = 2\pi - T_{\text{esc}}) \simeq \frac{\Delta_0}{2}\left(\frac{2eVT_{\text{esc}}}{\hbar}\right)^2 = 2\Delta_0\left(\frac{eV}{\Delta_0}\right)^{2/3} . \quad \text{(C.5)}$$

Here, $T_{\text{esc}} = \hbar(\Delta_0(eV)^2)^{-1/3}$ is the characteristic dissolution time of the Andreev states [89]. With this we define the characteristic velocity of the quasiparticle excitations $v_{qp} \simeq v_F(\delta E/\Delta_0)^{1/2}$ (v_F is the Fermi velocity) and the superconducting coherence length $\xi = \hbar v_F/\Delta_0 \gg L$. Having defined these quantities, we evaluate the characteristic distance δx travelled by the quasiparticle excitations during the period T_V and find $\delta x \sim \xi(\Delta_0/(eV))^{2/3} \gg \xi$. This implies that the excess energy released into the quasiparticle continuum is removed far from the nanowire junction during the period of the evolution of the Andreev states. Thus, no local heating of the junction is expected and the Andreev states are formed from the same quasiparticle distribution at the start of each period.

APPENDIX D

Supplement to Paper IV

Derivation of the system Hamiltonian

The Hamiltonian (equation (1) in Paper IV) can be derived starting from the classical equations of motion of the system. Referring to Fig.1 in Paper IV, these can be expressed as,

$$\frac{\partial \phi}{\partial t} = \frac{2eQ}{\hbar C} - \frac{4eLH}{\hbar}\dot{u}\,, \tag{D.1}$$

$$\frac{\partial Q}{\partial t} = I - \frac{2eE_J}{\hbar}\sin\phi\,, \tag{D.2}$$

$$m\ddot{u} = -ku + 2LH\left(\frac{2eE_J}{\hbar}\sin\phi\right)\,. \tag{D.3}$$

In the above, Q is the charge on the capacitor C such that the bias voltage over the junction is $V = Q/C$. In (D.1), the evolution of the phase-difference ϕ depends on the motion of the nanowire in the magnetic field ($\dot{u}$ is the velocity of the nanowire) which follows from the analysis of Paper II. Equation (D.2) gives the time rate of charge on the capacitor (note that the resistance R is not included here as it is treated as a perturbation to the evolution of the density matrix). Finally, equation (D.3) gives the equation of motion of the nanowire subject to the periodic driving force due to the alternating Josephson current over the junction. The corresponding system Hamiltonian reads,

$$\mathbb{H} = 4E_c n^2 - \frac{4eLH}{m}p_u n + \frac{8e^2L^2H^2}{m}n^2 + \frac{p_u^2}{2m} + \frac{ku^2}{2} - 4eLHj_0u - j\hbar\phi - E_J\cos\phi\,, \tag{D.4}$$

where $n = Q/(2e)$ is the number of Cooper pairs, $j = I/(2e)$ is the Cooper pair current and p_u is the momentum of the nanowire. Quantisation is achieved by regarding the variables u, p_u, ϕ and n as Hermitian operators satisfying the following commutation relations $[\hat{u}, \hat{p}_u]/\hbar = [\hat{\phi}, \hat{n}] = i$ and $[\hat{u}, \hat{\phi}] = [\hat{u}, \hat{n}] = [\hat{p}_u, \hat{\phi}] = [\hat{p}_u, \hat{n}] = 0$. With this we perform the unitary transformation,

$$\hat{\mathcal{H}} = e^{-i\Phi\hat{u}\hat{n}}\hat{\mathbb{H}}e^{i\Phi\hat{u}\hat{n}}\,, \tag{D.5}$$

after which the Hamiltonian reads,

$$\hat{\mathcal{H}} = 4E_c\hat{n}^2 - j\hbar\hat{\phi} - E_J\cos(\hat{\phi} - \Phi(\hat{b} + \hat{b}^\dagger)) + \hbar\omega\hat{b}^\dagger\hat{b}\,. \tag{D.6}$$

Note that in Paper IV, the notation $\hat{u} = \hat{b} + \hat{b}^\dagger$ is used for the deflection operator.

Resonance condition for the external bias current

By tuning the bias current the absorption channel, tunnelling through the absorption of a mechanical vibron, can be brought into resonance, which greatly promotes the cooling process. The condition under which this can be achieved can be found following the analysis outlined in Ref. [82].

Mathematically, the motion of the phase in the tilted washboard potential $U(\hat{\phi})$ is described by the Hamiltonian,

$$\hat{\mathcal{H}}_{TW} = 4E_c\hat{n}^2 + U(\hat{\phi})\,, \qquad U(\hat{\phi}) = -E_J\cos\hat{\phi} - j\hbar\hat{\phi}\,. \tag{D.7}$$

In (D.7), the charging energy E_c can be thought of as the inverse mass of the classical particle moving in the equivalent potential. Under the condition $4E_c/E_J \ll 1$, equation (D.7) corresponds to that of a classical particle which is highly localised to the minima of the potential $U(\hat{\phi})$.

Rewriting (D.7) in units of $\hbar\omega_p/2$, and separating out the harmonic and anharmonic parts one finds the full set of unperturbed energy levels (harmonic part of the Hamiltonian),

$$\begin{aligned} F_{l,m} &= E^0_m - 2\pi s l\nu\,, \\ E^0_m = -\nu + 2m + 1\,, &\qquad \nu = \sqrt{\frac{E_J}{2E_c}} > 1\,, \qquad s = \frac{\hbar I}{2eE_J}\,. \end{aligned} \tag{D.8}$$

To derive the above equation we have used $\hat{n} = -i\partial_{\hat{\phi}}$ which follows from the commutation relation $[\hat{\phi}, \hat{n}] = i$. Equation (D.8) gives unperturbed (parabolic) quantised energy levels for the electronic degrees of freedom inside each valley l where $m = 0, 1, 2, ...$ In Paper IV, we consider only the two lowest energy levels $m = 0, 1$ and furthermore restrict our analysis to neglect with corrections to $F_{l,m}$ from the anharmonic parts of the Hamiltonian. With these considerations, the eigenvalues for the electronic degrees of freedom (in real units) in the basis $|l, \sigma\rangle$ are $\mathcal{F}_{l,\sigma} = \hbar\omega_p m_\sigma - l\pi\hbar I/e$ as stated in Paper IV. With these assumptions the absorption channel is resonant, $F_{l,0} = F_{l+1,1} - 2\omega/\omega_p$, when the junction is biased at the current $s_0 = \frac{1}{\pi\nu}(1 - \omega/\omega_p)$. The corresponding expression in real units is then,

$$I_0 = \frac{e\omega_p}{\pi}\left(1 - \frac{\omega}{\omega_p}\right)\,, \tag{D.9}$$

as stated in Paper IV.

To extend the analysis to account also for the anharmonic parts of the tilted washboard Hamiltonian, we perform a perturbation calculation to order ν^{-2} to find the corrections $\Delta E_m(s_0)$ to the unperturbed energy levels, $E^0_m = E_m - \Delta E_m(s_0)$. Substituting E_m for the unperturbed energy levels in (D.8) we find

the conditions for the bias current under which the system is resonant through the absorption channel,

$$s = \frac{1}{\pi\nu}\left(\left(1-\frac{\omega}{\omega_p}\right) - \frac{1}{4\nu} - \frac{\left(1-\frac{\omega}{\omega_p}\right)^2}{4\pi^2\nu^2} - \frac{1}{16\nu^2}\right) \simeq \frac{1}{\pi\nu}\left(1-\frac{\omega}{\omega_p}\right) . \quad \text{(D.10)}$$

Including the corrections from the anharmonic parts of the potential, we find that the inter-level energy spacing within a valley is not constant. This conditions ensures that we may neglect with the higher $m \geq 2$ states as these will be far (on the energy scale of $\hbar\omega$) from resonance under bias current conditions $I \simeq I^*$.

BIBLIOGRAPHY

[1] R. P. Feynman, "*There's Plenty of Room at the Bottom*", Engineering and Science Magazine **23**, 22 (1960).

[2] Project of Emerging Nanotechnologies, April, 2008. http://www.nanotechproject.org/news/archive/6697.

[3] E. Pop, "*Energy Dissipation and Transport in Nanoscale Devices*", Nano Res. **3**, 147 (2010).

[4] H-Y. Chiu, P. Hung, H. W. Postma, and M. Bockrath, "*Atomic-Scale Mass Sensing Using Carbon Nanotube Resonators*", Nano Lett. **8**, 4342 (2008).

[5] K. Jensen, K. Kim, and A. Zettl, "*An atomic-resolution nanomechanical mass sensor*", Nat. Nanotechnol. **3**, 533 (2008).

[6] B. Lassagne, D. Garcia-Sanchez, A. Aguasca, and A. Bachtold, "*Ultasensitive Mass Sensing with a Nanotube Electromechanical Resonator*", Nano Lett. **8**, 3735 (2008).

[7] A. K. Naik, M. S. Hanay, W. K. Hiebert, X. L. Feng, and M. L. Roukes, "*Towards single-molecule nanomechanical mass spectrometry*", Nat. Nanotechnol. **4**, 445 (2009).

[8] M. P. Blencowe, "*Nanoelectromechanical systems*", Contemp. Phys. **46**, 249 (2005).

[9] M. L. Roukes, "*Nanoelectromechanical systems face the future*", Phys. World **14**, 25 (2001).

[10] M. L. Roukes, "*Nanoelectromechanical Systems*", Technical digest of the 2000 solid-state sensor and actuator workshop, Clevland (2000).

[11] K. C. Schwab and M. L. Roukes, "*Putting Mechanics into Quantum Mechanics*", Phys. Today **58**, 36 (2005), no. 7.

[12] A. D. O'Connell et al., "*Quantum ground state and single-phonon control of a mechanical resonator*", Nature **464**, 697 (2010).

[13] B. Abbott et al., "*Observation of a kilogram-scale oscillator near its quantum ground state*", New J. Phys. **11**, 073032 (2009).

[14] I. Martin, A. Shnirman, L. Tian, and P. Zoller, "*Ground-state cooling of mechanical resonators*", Phys. Rev. B **69**, 125339 (2004).

[15] I. Wilson-Rae, P. Zoller, and A. Imamoğlu, "*Laser Cooling of a Nanomechanical Resonator Mode to its Quantum Ground State*", Phys. Rev. Lett. **92**, 075507 (2004).

[16] A. Naik, O. Buu, M. D. LaHaye, A. D. Armour, A. A. Clerk, M. P. Blencowe, and K. C. Schwab, "*Cooling a nanomechanical resonator with quantum back-action*", Nature **443**, 193 (2006).

[17] T. Rocheleau, T. Ndukum, C. Macklin, J. B. Hertzberg, A. A. Clerk, and K. C. Schwab, "*Preparation and detection of a mechanical resonator near the ground state of motion*", Nature **463**, 72 (2009).

[18] S. H. Ouyang, J. Q. You, and F. Nori, "*Cooling a mechanical resonator via coupling to a tunable double quantum dot*", Phys. Rev. B **79**, 075304 (2009).

[19] S. Zippilli, G. Morigi, and A. Bachtold, "*Cooling Carbon Nanotubes to the Phononic Ground State with a Constant Electron Current*", Phys. Rev. Lett. **102**, 096804 (2009).

[20] S. Zippilli, A. Bachtold, and G. Morigi, "*Ground-state cooling vibrations of suspended carbon nanotubes with constant electron current*", Phys. Rev. B **81**, 205408 (2010).

[21] A. Schliesser, R. Rivière, G. Anetsberger, O. Arcizet, and T. J. Kippenberg, "*Resolved-sideband cooling of a micromechanical resonator*", Nat. Phys. **4**, 415 (2008).

[22] T. J. Kippenberg and K. J. Vahala, "*Cavity Optomechanics: Back-action at the Mesoscale*", Science **321**, 1172 (2008).

[23] F. Marquardt and S. M. Girvin, "*Optomechanics*", Physics **2**, 40 (2009).

[24] M. Poot, *Mechanical systems at the nanoscale*. PhD thesis, Delft Univesity of Technology, 2009.

[25] R. G. Knobel and A. N. Cleland, "*Nanometer-scale displacement sensing using a single elecron transistor*", Nature **424**, 291 (2003).

[26] M. D. LaHaye, O. Buu, B. Camarota, and K. C. Schwab, "*Approaching the Quantum Limit of a Nanomechanical Resonator*", Science **304**, 74 (2004).

[27] S. Etaki, M. Poot, I. Mahboob, K. Onomitsu, H. Yamaguchi, and H. S. J. van der Zant, "*Motion detection of a micromechanical resonator embedded in a d.c. SQUID*", Nat. Phys. **4**, 785 (2008).

[28] J. D. Teufel, T. Donner, M. A. Castellanos-Beltran, J. W. Harlow, and K. W. Lehnert, "*Nanomechanical motion measured with an imprecision below that at the standard quantum limit*", Nature Nanotechnol. **4**, 820 (2009).

[29] M. Aspelmeyer and K. C. Schwab, "*Focus on Mechanical Systems at the Quantum Limit*", New J. Phys. **10**, 095001 (2008).

[30] B. D. Josephson, "*Possible new effects in superconductive tunnelling*", Phys. Lett. **1**, 251 (1962).

[31] L. N. Cooper, "*Bound Electron Pairs in a Degenerate Fermi Gas*", Phys. Rev. **104**, 1189 (1956).

[32] A. Barone and G. Paterno, *Physics and Applications of the Josephson Effect*. John Wiley & Sons, New York, 1982.

[33] M. Tinkham, *Introduction to Superconductivity*. Dover Publications, Mineola, 2nd ed., 1996.

[34] R. P. Feynman, R. B. Leighton, and M. Sands, *The Feynman Lectures on Physics*, vol. 3. Addison-Wesley Publishing, Reading, 1965.

[35] J. Bardeen, L. N. Cooper, and J. R. Schrieffer, "*Microscopic Theory of Superconductivity*", Phys. Rev. **106**, 162 (1957).

[36] J. Bardeen, L. N. Cooper, and J. R. Schrieffer, "*Theory of Superconductivity*", Phys. Rev. **108**, 1175 (1957).

[37] A. F. Andreev, "*The thermal conductivity of the intermediate state in superconductors*", Sov. Phys. JETP **19**, 1228 (1964).

[38] C. W. J. Beenakker, *Why does a metal-superconductor junction have a resistance?* Kluwer Academic Publishers, Amsterdam, 2000.

[39] N. I:son Lundin, *Adiabatic Andreev Levels Under Irradiation - Coherent Dynamics and Dephasing*. PhD thesis, Chalmers University of Technology, 2000.

[40] P. F. Bagwell, "*Suppression of the Josephson current through a narrow, mesoscopic, semiconductor channel by a single impurity*", Phys. Rev. B **46**, 12573 (1992).

[41] C. W. J. Beenakker, "*Universal Limit of Critical-Current Fluctuations in Mesoscopic Josephson Junctions*", Phys. Rev. Lett. **67**, 3836 (1991).

[42] S. De Franceschi, L. Kouwenhoven, C. Schönenberger, and W. Wernsdorfer, "*Hybrid superconductor-quantum dot devices*", Nat. Nanotechnol. **5**, 703 (2010).

[43] A. Yu. Kasumov et al., "*Supercurrents Through Single-Walled Carbon Nanotubes*", Science **284**, 1508 (1999).

[44] H. I. Jørgensen, K. Grove-Rasmussen, T. Novotný, K. Flensberg, and P. E. Lindelof, "*Electron Transport in Single-Wall Carbon Nanotube Weak Links in the Fabry-Perot Regime*", Phys. Rev. Lett. **96**, 207003 (2006).

[45] P. Jarillo-Herrero, J. A. van Dam, and L. P. Kouwenhoven, "*Quantum supercurrent transistors in carbon nanotubes*", Nature **439**, 953 (2006).

[46] M. Ferrier, A. Kasumov, R. Deblock, S. Guéron, and H. Bouchiat, "*Superconducting properties of carbon nanotubes*", C. R. Phys. **10**, 252 (2009).

[47] W. Belzig, "*Hybrid superconducting devices: Bound in a nanotube*", Nat. Phys. **6**, 940 (2010).

[48] J-D. Pillet, C. H. L. Quay, P. Morfin, C. Bena, A. Levy Yeyati, and P. Joyez, "*Andreev bound states in supercurrent-carrying carbon nanotubes revealed*", Nat. Phys. **6**, 965 (2010).

[49] M. M. J. Treacy, T. W. Ebbesen, and J. M. Gibson, "*Exceptionally high Young's modulus observed for individual carbon nanotubes*", Nature **381**, 678 (1996).

[50] E. W. Wong, P. E. Sheehan, and C. M. Lieber, "*Nanobeam Mechanics: Elasticity, Strength, and Toughness of Nanorods and Nanotubes*", Science **277**, 1971 (1997).

[51] Z-P. Yang, L. Ci, J. A. Bur, S-Y. Lin, and P. M. Ajayan, "*Experimental Observation of an Extremely Dark Material Made By a Low-Density Nanotube Array*", Nano Lett. **8**, 446 (2008).

[52] L. Hu, J. W. Choi, Y. Yang, S. Jeong, F. La Mantia, L-F. Cui, and Y. Cui, "*Highly conductive paper for energy-storage devices*", P. Natl. Acad. Sci. USA **106**, 21490 (2009).

[53] L. Hu et al., "*Stretchable, Porus, and Conductive Energy Textiles*", Nano Lett. **10**, 708 (2010).

[54] L. Qu, L. Dai, M. Stone, Z. Xia, and Z. L. Wang, "*Carbon Nanotube Arrays with Strong Shear Binding-On and Easy Normal Lifting-Off*", Science **322**, 238 (2008).

[55] S. W. Lee et al., "*High-power lithium batteries from functionalized carbon-nanotube electrodes*", Nat. Nanotechnol. **5**, 531 (2010).

[56] K. Mylvaganam and L. C. Zhang, "*Energy absorption capacity of carbon nanotubes under ballistic impact*", Appl. Phys. Lett. **89**, 123127 (2006).

[57] A. Barreiro, R. Rurali, E. R. Hernández, J. Moser, T. Pichler, L. Forró, and A. Bachtold, "*Subnanometer Motion of Cargoes Driven by Thermal Gradients Along Carbon Nanotubes*", Science **320**, 775 (2008).

[58] G. E. Begtrup, W. Gannett, T. D. Yuzvinsky, V. H. Crespi, and A. Zettl, "*Nanoscale Reversible Mass Transport for Archival Memory*", Nano Lett. **9**, 1835 (2009).

[59] J. Cumings and A. Zettl, "*Low-Friction Nanoscale Linear Bearing Realized from Multiwall Carbon Nanotube*", Science **289**, 602 (2000).

[60] K. Jensen, J. Weldon, H. Garcia, and A. Zettl, "*Nanotube Radio*", Nano Lett. **7**, 3508 (2007).

[61] M. S. Arnold, A. A. Green, J. F. Hulvat, S. I. Stupp, and M. C. Hersam, "*Sorting carbon nanotubes by electronic structure using density differentiation*", Nat. Nanotechnol. **1**, 60 (2006).

[62] T. Tanaka et al., "*Simple and Scalable Gel-Based Separation of Metallic and Semiconducting Carbon Nanotubes*", Nano Lett. **9**, 1497 (2009).

[63] V. Sazonova, Y. Yaish, H. Üstünel, D. Roundy, T. A. Arias, and P. L. McEuen, "*A tunable carbon nanotube electromechanical oscillator*", Nature **431**, 284 (2004).

[64] A. K. Hüttel, G. A. Steele, B. Witkamp, M. Poot, L. P. Kouwenhoven, and H. S. J. van der Zant, "*Carbon Nanotubes as Ultrahigh Quality Factor Mechanical Resonators*", Nano Lett. **9**, 2547 (2009).

[65] D. Garcia-Sanchez, A. San Paulo, M. J. Esplandiu, F. Perez-Murano, L. Forró, A. Aguasca, and A. Bachtold, "*Mechanical Detection of Carbon Nanotube Resonator Vibrations*", Phys. Rev. Lett. **99**, 085501 (2007).

[66] A. K. Hüttel, M. Poot, B. Witkamp, and H. S. J. van der Zant, "*Nanoelectromechanics of suspended carbon nanotubes*", New J. Phys. **10**, 095003 (2008).

[67] P. Avouris, J. Appenzeller, R. Martel, and S. J. Wind, "*Carbon Nanotube Electronics*", P. IEEE **91**, 1772 (2003).

[68] P. Avouris, "*Supertubes*", IEEE Spectrum **41**, 40 (2004).

[69] P. L. McEuen, M. S. Fuhrer, and H. Park, "*Single-Walled Carbon Nanotube Electronics*", IEEE Transactions on Nanotechnology **1**, 78 (2002).

[70] R. I. Shekhter, F. Santandrea, G. Sonne, L. Y. Gorelik, and M. Jonson, "*Nonequilibrium and quantum coherent phenomena in the electromechanics of suspended nanowires*", Low Temp. Phys. **35**, 662 (2009).

[71] G. Sonne, M. E. Peña-Aza, L. Y. Gorelik, R. I. Shekhter, and M. Jonson, "*Voltage-driven superconducting weak link as a refrigerator for cooling of nanomechanical vibrations*", Low Temp. Phys. **36**, 902 (2010).

[72] H. Park, J. Park, A. K. L. Lim, E. H. Anderson, A. P. Alivisatos, and P. L. McEuen, "*Nanomechanical oscillations in a singe-C_{60} transistor*", Nature **407**, 57 (2000).

[73] J. Koch and F. von Oppen, "*Franck-Condon Blockade and Giant Fano Factors in Transport through Single Molecules*", Phys. Rev. Lett. **94**, 206804 (2005).

[74] S. Sapmaz, P. Jarillo-Herrero, Y. M. Blanter, C. Dekker, and H. S. J. van der Zant, "*Tunneling in Suspended Carbon Nanotubes Assisted by Longitudinal Phonons*", Phys. Rev. Lett. **96**, 026801 (2006).

[75] G. Sonne, L. Y. Gorelik, R. I. Shekhter, and M. Jonson, "*High-temperature excess current and quantum suppression of electronic backscattering*", Europhys. Lett. **84**, 27002 (2008).

[76] R. Leturcq et al., "*Franck-Condon blockade in suspended carbon nanotube quantum dots*", Nat. Phys. **5**, 327 (2009).

[77] A. K. Hüttel, B. Witkamp, M. Leijnse, M. R. Wegewijs, and H. S. J. van der Zant, "*Pumping of Vibrational Excitations in the Coulomb-Blockade Regime in a Suspended Carbon Nanotube*", Phys. Rev. Lett. **102**, 225501 (2009).

[78] R. I. Shekhter, L. Y. Gorelik, L. I. Glazman, and M. Jonson, "*Electronic Aharanov-Bohm Effect Induced by Quantum Vibrations*", Phys. Rev. Lett. **97**, 156801 (2006).

[79] E. Buks and M. P. Blencowe, "*Decoherence and recoherence in a vibrating rf SQUID*", Phys. Rev. B **74**, 174504 (2006).

[80] E. Buks, E. Segev, S. Zaitsev, B. Abdo, and M. P. Blencowe, "*Quantum nondemolition measurement of discrete Fock states of a nanomechanical resonator*", Europhys. Lett. **81**, 10001 (2008).

[81] M. Poot, S. Etaki, I. Mahboob, K. Onomitsu, H. Yamaguchi, Ya. M. Blanter, and H. S. J. van der Zant, "*Tunable Backaction of a DC SQUID on an Integrated Micromechanical Resonator*", Phys. Rev. Lett. **105**, 207203 (2010).

[82] J. M. Schmidt, A. N. Cleland, and J. Clarke, "*Resonant tunneling in small current-biased Josephson junctions*", Phys. Rev. B **43**, 229 (1991).

[83] J. M. Martinis, M. H. Devoret, and J. Clarke, "*Energy-Level Quantization in the Zero-Voltage State of a Current-Biased Josephson Junction*", Phys. Rev. Lett. **55**, 1543 (1985).

[84] S. Han, Y. Yu, X. Chu, S-I. Chu, and Z. Wang, "*Time-Resolved Measurement of Dissipation-Induced Decoherence in a Josephson Junction*", Science **293**, 1457 (2001).

[85] Y. Yu, S. Han, X. Chu, S-I. Chu, and Z. Wang, "*Coherent Temporal Oscillations of Macroscopic Quantum States in a Josephson Junction*", Science **296**, 889 (2002).

[86] D. Esteve, M. H. Devoret, and J. M. Martinis, "*Effect of an arbitrary dissipative circuit on the quantum energy levels and tunneling of a Josephson junction*", Phys. Rev. B **34**, 158 (1986).

[87] D. Fedorets, *Quantum Theory of Nanoelectromechanical Shuttling*. PhD thesis, Chalmers University of Technology, 2004.

[88] A. Zazunov, D. Feinberg, and T. Martin, "*Phonon-mediated negative differential conductance in molecular quantum dots*", Phys. Rev. B **73**, 115405 (2006).

[89] L. Y. Gorelik, N. I. Lundin, V. S. Shumeiko, R. I. Shekhter, and M. Jonson, "*Superconducting Single-Mode Contact as a Microwave-Activated Quantum Interferometer*", Phys. Rev. Lett. **81**, 2538 (1998).